Technical Report

TR-10-65

Thermo-hydro-geochemical modelling of the bentonite buffer

LOT A2 experiment

Clara Sena, Joaquin Salas, David Arcos
Amphos 21 Consulting S.L. Spain

December 2010

Svensk Kärnbränslehantering AB
Swedish Nuclear Fuel
and Waste Management Co

Box 250, SE-101 24 Stockholm
Phone +46 8 459 84 00

ISSN 1404-0344
SKB TR-10-65

Thermo-hydro-geochemical modelling of the bentonite buffer

LOT A2 experiment

Clara Sena, Joaquin Salas, David Arcos
Amphos 21 Consulting S.L. Spain

December 2010

Abstract

The Swedish Nuclear Fuel and waste management company (SKB) is conducting a series of long term buffer material (LOT) tests at the Äspö Hard Rock Laboratory (HRL) to test the behaviour of the bentonite buffer under conditions similar to those expected in a KBS-3 deep geological repository for high level nuclear waste (HLNW).

In the present work a numerical model is developed to simulate (i) the thermo-hydraulic, (ii) transport and (iii) geochemical processes that have been observed in the LOT A2 test parcel. The LOT A2 test lasted approximately 6 years, and consists of a 4 m long vertical borehole drilled in diorite rock, from the ground of the Äspö HRL tunnel. The borehole is composed of a central heater, maintained at 130°C in the lower 2 m of the borehole, a copper tube surrounding the heater and a 100 mm thick ring of pre-compacted Wyoming MX-80 bentonite around the copper tube /Karnland et al. 2009/.

The numerical model developed here is a 1D axis-symmetric model that simulates the water saturation of the bentonite under a constant thermal gradient; the transport of solutes; and, the geochemical reactions observed in the bentonite blocks. Two cases have been modelled, one considering the highest temperature reached by the bentonite (at 3 m depth in the borehole, where temperatures of 130 and 85°C have been recorded near the copper tube and near the granitic host rock, respectively) and the other case assuming a constant temperature of 25°C, representing the upper part of borehole, where the bentonite has not been heated.

In the LOT A2 test, the initial partially saturated bentonite becomes progressively water saturated, due to the injection of Äspö granitic groundwater at granite – bentonite interface. The transport of solutes during the bentonite water saturation stage is believed to be controlled by water uptake from the surrounding groundwater to the wetting front and, additionally, in the case of heated bentonite, by a cyclic evaporation/condensation process /Karnland et al. 2009/. Once bentonite is water saturated, the transport of solutes is driven by diffusion.

Although Donnan equilibrium /Birgersson and Karnland 2009/ and anion exclusion /Muurinen et al. 2004/ are able to influence the mobility of chloride in the bentonite buffer, under the high temperature LOT A2 test conditions, measured data seem to indicate a relatively low influence of these processes on the transport of chloride. For this reason, the transport of chloride has been modelled taking into account advective, dispersive and diffusive fluxes that are believed to have occurred in the LOT A2 test.

Numerical results were conducted at fixed thermal gradients for both heated and non-heated bentonite based on the temperatures recorded during the experiment for both heated and non-heated bentonite. The computed evolution of the bentonite saturation indicates that, within approximately one year, the bentonite blocks located at the depth of the heater are completely water saturated which agrees with measured data. The simulated transport of chloride is also in good agreement with data measured at the end of the LOT A2 test for the two cases considered, reflecting the reliability of the conceptual model defined for the LOT A2 test.

Based on the geochemical data obtained at end of the LOT A2 test, and on previous modelling exercises /Arcos et al. 2006/, the main geochemical processes that are believed to have developed during the LOT A2 test are: (i) precipitation/dissolution of carbonate, sulphate and silica minerals and, (ii) cation exchange in the montmorillonite interlayer. Numerical results predict the dissolution – precipitation of anhydrite, calcite and silica in the heated bentonite in agreement with data measured at the end of the LOT A2 test.

Sammanfattning

Svensk Kärnbränslehantering AB (SKB) genomför en serie av långtidstester av buffertmaterial (LOT) i Äspölaboratoriet för att studera utvecklingen i bentonitbufferten under förhållanden liknande till de som råder i ett KBS-3 förvar för använt kärnbränsle.

I denna studie har en numerisk modell utvecklats för att simulera: (i) de termohydrauliska, (ii) transport och (iii) geokemiska processerna som har observerats i LOT A2 paketet. LOT A2 pågick under ungefär sex år och består av ett 4 meter djupt vertikalt hål borrat i diorit, från golvet i tunneln i Äspölaboratoriet. I borrhålet finns en central värmare, vilken har hållits vid 130 °C i den nedre halvan. Runt värmaren sitter ett kopparrör som omges av kompakterad MX-80 bentonit med radien 100 mm /Karnland et al. 2009/.

Den numeriska modellen som utvecklats här är en 1D axi-symetrisk modell som simulerar: vattenmättnaden av bentoniten under en konstant termisk gradient, transporten av lösta ämnen och de geokemiska reaktionerna som har observerats i bentonitblocken. Två fall har modellerats: ett som tar hänsyn till de högsta temperaturer som har uppmätts (på 3 meters djup där temperaturer på 130 °C och 85 °C har uppmätts nära kopparröret respektive berget) och ett fall där en konstant temperatur av 25 °C vilket respresenterar den över delen av borrhålet, där bentoniten inte har varit uppvärmd.

I LOT A2 testet blir den initialt delvis mättade bufferten successivt vattenmättad, genom att Äspögrundvatten tränger in från gränsskiktet berg-buffert. Transporten av lösta specier tros vara styrd av upptag av vatten från det omgivande berget till mättnadsfronten och, i fallet med den uppvärmda bentoniten, av en cyklisk förångnings/kondensationsprocess /Karnland et al. 2009/. När bentoniten är mättad drivs transporten av lösta specier med diffusion.

Donnanjämvikt /Birgersson and Karnland 2009/ och anjonexklusion /Muurinen et al. 2004/ skulle potentiellt kunna influera transporten av kloridjoner i en bentonitbuffert. Mätta data från högtemperaturtesten i LOT A2 tyder dock på att dessa mekanismer skulle ha relativt lite betydelse för transporten av klorid. Av det skälet så har transporten av klorid modellerats enbart med de advektiva, diffusiva och dispersiva flöden som förväntas ha förekommit i LOT A2.

Numeriska resultat har producerats för fixerade temperaturgradienter, både för uppvärmda och ouppvärmda förhållanden. Gradienterna är baserade på uppmätta temperaturer från experimentet. Den beräknade vattenmättnaden av bentoniten visar att blocken runt värmaren i den nedre delen är fullt mättade efter ungefär ett år, vilket stämmer väl överens med mätta data. Simuleringen av transporten av klorid stämmer också väl överens med mätningarna vid försökets avslut för båda de beräknade fallen. Detta ger en indikation om modellens pålitlighet.

Baserat på geokemiska data från brytningen av LOT A2 tillsammans med tidigare modelleringsinsatser /Arcos et al. 2006/, är slutsatsen att de huvudsakliga geokemiska processerna som har påverkat utveckling i LOT A2 är: (i) upplösning/utfällning av karbonat, sulfat och kiselmineral, (ii) katjonbyte i montmorillonitens ytlager. De numeriska beräkningarna av upplösning utfällning av anhydrit, kalcit och kisel i den uppvärmda bentoniten överensstämmer med data från brytningen av LOT A2.

Contents

1 Introduction

1.1 Motivation and context

The Swedish Nuclear Fuel and waste management company (SKB) is conducting a series of long term buffer material (LOT) tests, at the Äspö Hard Rock Laboratory (HRL), to check hypotheses for the evolution and behaviour of the bentonite buffer under conditions similar to those in a KBS-3 deep geological repository for high level nuclear waste (HLNW).

The LOT test series comprise 7 parcels, which are run for 1, 5 and 20 years. This report concerns the development of a numerical model that accounts for non-isothermal, variably saturated flow, coupled with geochemical reactions, to reproduce data measured at one of the 5 years experiment; the LOT A2 test parcel.

The LOT A2 test parcel was placed in a core-drilled borehole (drilled from the ground of the tunnel of Äspö HRL), in the granitic rock at a depth of 450 m below the topographic surface. The parcel modelled in this work is composed by a central heater surrounded by a copper tube, and 100 mm of compacted bentonite placed between the copper tube and the diorite rock. The heater is intended to reproduce the decay power from the HLNW. It should be noted that the highest temperature expected for the canisters in a KBS-3 repository is 90°C. Nevertheless, in order to assess the adverse consequences of a higher temperature, the heater in the A2 test parcel has been set to a temperature of 130°C in the lower 2 m of the borehole /Karnland et al. 2009/.

Measured distribution of ion and water content in the bentonite samples, after the 5 years test, point to the hypothesis that a cyclic evaporation/condensation process has been established in the heated bentonite. This evaporation/condensation cycle has lead to an overall salt enrichment at the vicinity of the heated copper tube /Karnland et al. 2009/.

The numerical model developed here aims at simulating the saturation of the bentonite under both isothermal and non-isothermal conditions, accounting for evaporation and condensation of water, together with geochemical reactions between solutes and bentonite minerals.

1.2 Objectives

The main objective of the present work is to develop a hydro-thermal-geochemical model of the experimental parcel A2 of the LOT project, based on the mineralogical and porewater chemical composition obtained up to date, and also on previous modelling exercises /Arcos et al. 2006/. In addition, this model is intended to provide insights into the effect of thermo-hydraulic processes induced by the heater, such as evaporation and condensation, on the geochemical behaviour of the compacted bentonite and on the corresponding porewater composition.

The LOT A2 parcel consists in several bentonite blocks that surround the copper tube from 4 m depth to the top of the borehole. The heater that induced the thermal gradient during the LOT A2 experiment was placed in the lower 2 m of the borehole. This means that the highest thermal gradient was established in the bentonite blocks located at around 3 m depth.

Since the objective of the present work is to assess the influence of the thermo-hydraulic processes on the geochemical behaviour of the bentonite, the numerical model built here is focused on the standard bentonite blocks (i.e. without additives) located at a depth of 3 m, where the highest thermal gradient was registered, and the comparison of the results with the model for the bentonite at 1 m depth, where lower temperatures prevailed (Figure 2-1).

1.3 Scope

The work presented here concerns the development of numerical simulations of selected blocks of the LOT A2 test /Karnland et al. 2009/ which help us to improve our knowledge and validate the hypotheses stated for the thermo-hydraulic, transport and geochemical processes that prevail during the hydration of the bentonite buffer in a KBS-3 deep geological repository.

In Chapter 2 the LOT A2 test is briefly described by pointing out the main aspects of the experiment that will influence the initial and boundary conditions of the corresponding numerical simulations. Then, the conceptual model of the thermo-hydraulic, transport and geochemical processes that are believed to occur in the bentonite buffer of a KBS-3 deep geological repository is presented in Chapter 3. In order to validate our conceptual model, an additional numerical model developed for a laboratory experiment conducted by CIEMAT using the FEBEX bentonite /Villar et al. 2008a/ is also described in Chapter 3.

The setup of the numerical simulations developed for the LOT A2 test is described in Chapter 4 which is followed by the detailed analysis and discussion of the modelling results, in Chapter 5. In Chapter 6, the main conclusions achieved in this work are presented.

2 LOT A2 test

The LOT test parcels contain prefabricated bentonite blocks placed around a copper tube, which is placed in vertical boreholes in the granitic rock. After exposure to field conditions for a defined period of time, the parcel is extracted by overcore drilling around the original borehole, and the whole test parcel is lifted and split. Material from defined positions of the parcel is thereafter examined by well-defined tests and analyses in order to provide data for the different objectives /Karnland et al. 2009/.

2.1 Description of the LOT A2 test

2.1.1 Geometry and thermo-hydraulic conditions

The LOT A2 test consists of a 4 m-long vertical borehole core-drilled in diorite rock, from the ground of the Äspö HRL tunnel. The depth from surface is around 450 m, and the rock consists mainly of Äspö diorite, which is crossed by some pegmatite dikes and bands of fine-grained granite.

The borehole of the LOT A2 test parcel is composed of a central heater located in the lower 2 m of the borehole and maintained at 130°C (which corresponds to a constant heater power of 850 W). A copper tube of 100 mm diameter surrounds the heater and, between the copper tube and the diorite rock, a 100 mm thick ring of pre-compacted Wyoming MX-80 bentonite is placed (Figure 2-1). The duration time of the LOT A2 test parcel was more or less six years:

- first year, during which temperature of the bentonite progressively increased towards a stable temperature profile; and,
- further five years, where the thermal gradient was kept stable /Karnland et al. 2000/.

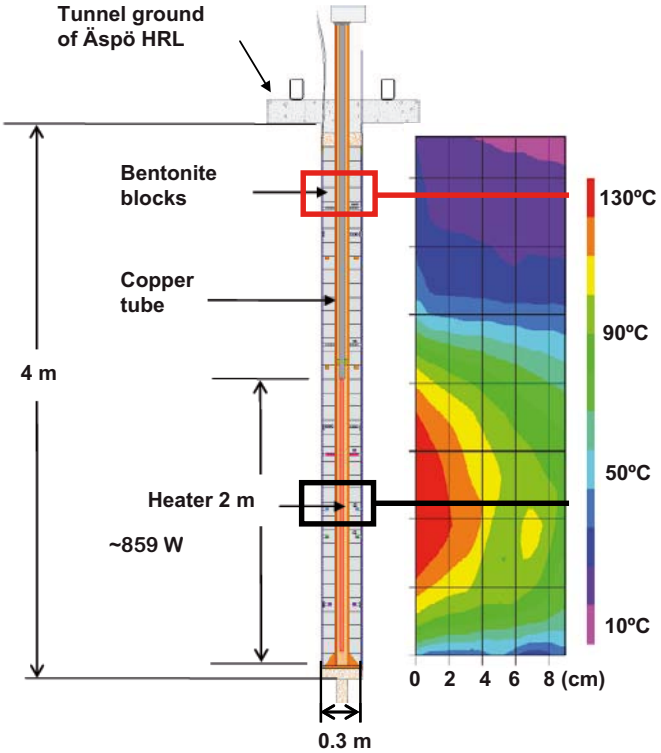

Figure 2-1. *Vertical cross section of the LOT A2 test parcel built at the Äspö HRL, and the resulting thermal field. The non-isothermal bentonite block modelled in this work is identified with a black rectangle, and the isothermal bentonite block (25°C) is identified with a red rectangle (modified with permission from /Karnland et al. 2000/).*

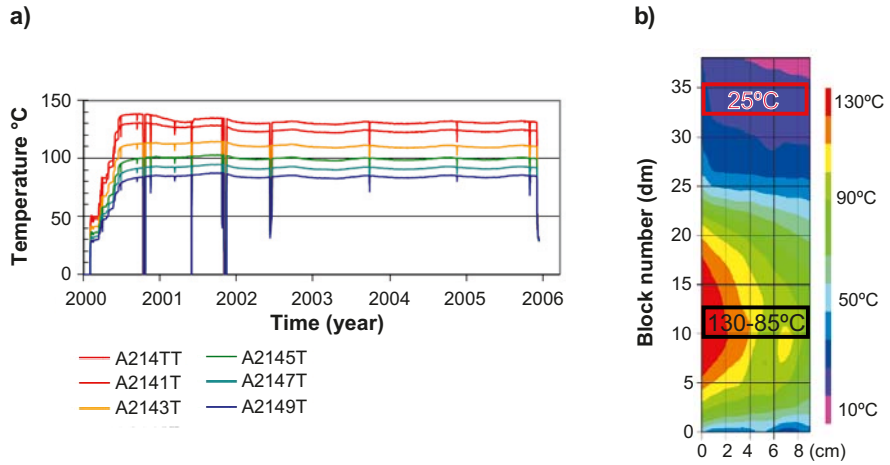

Figure 2-2. *a) Time evolution of temperature in the bentonite ring, in the sensor-id A214TT (at a depth of 2.6 m from the top of the borehole). A214TT is located at the copper tube surface and the underlying curves correspond to points successively 2 cm closer to the rock. The lowest curve represents a point approximately 1 cm from the rock; b) Temperature distribution at termination of the heating which represents the major part (at least the last five years) of the duration of the LOT A2 test parcel (modified from /Karnland et al. 2009/). Location of the bentonite block that is modelled here is highlighted with a black rectangle.*

The thermal conditions of the LOT A2 parcel were built gradually, from February 2000 until June 2000. The heater was placed at the bottom of the borehole and has a length of 2 m. It was regulated to give a constant power of 850 W, so that the temperature of the bentonite at the interface with the copper tube around the heater location was 130°C (Figure 2-2), and 85°C at the interface with the granitic rock /Karnland et al. 2000/.

Temperature, total pressure, water pressure and water content were measured during the heating period. The sensors were connected to a standard PC-based data acquisition system, and registrations were made regularly every hour /Karnland et al. 2009/.

During the first year of the LOT A2 test parcel, temperature in the bentonite buffer progressively increased, as the heater power increased (Figure 2-2a), towards a stable profile that was kept more or less constant throughout the subsequent five years of the test (Figure 2-2b). During these last five years no overheating or temperature drops took place /Karnland et al. 2009/. The numerical model developed here doesn't consider the heating period, and a constant thermal gradient has been implemented during the five years of calculations. In this way, the numerical profile of temperatures in the bentonite buffer shows a constant thermal gradient and a significant stability over time.

All moisture sensors operating during the LOT A2 test indicated a considerably fast increase in humidity to over 90% within the first year /Karnland et al. 2009/, meaning that during most of the experiment the bentonite was almost fully water saturated.

2.1.2 Hydrochemical conditions

Some bentonite blocks used in the LOT A2 test parcel were previously analysed for several hydro-geochemical and physical parameters. These blocks are called the reference bentonite blocks and the data obtained from such analyses represent the initial conditions prior to the heating and water saturation of the LOT A2 test.

The water composition of the reference bentonite porewater (A213) is obtained from aqueous leachates extracted from the bentonite used to build the LOT A2 bentonite rings. These aqueous leachates are obtained by dispersion of bentonite in deionised water, in a solid/liquid ratio of 1/10.

The chemical composition of the aqueous leachate from the reference sample A213 (Table 2-1) is taken from the aqueous leachates performed by the Rock-Water Interaction Group at the University of Bern /Karnland et al. 2009/. Preliminary calculations performed from the aqueous leachates obtained from the reference samples A2(1-5)Rb have been discarded, because the chemical data has

Table 2-1. (1) Leachate values for sample LOT A213 from UniBern as reported in /Karnland et al. 2009/ (water concentrations for a solid/liquid ratio of 1/10). (2) Calculated initial porewater concentrations from leachate data of UniBern. (3) Corrected porewater concentration calculated in equilibrium with (i) the composition of the cation exchanger as reported in /Karnland et al. 2009/; (ii) gypsum and calcite; and, (iii) atmospheric partial pressure of CO_2 and O_2.

Sample LOT A213	Concentrations (mol·L^{-1})		
	*(1)	(2)	(3)
pH	9.19	9.19	7.859
Na	$1.33\cdot10^{-2}$	$1.33\cdot10^{0}$	$2.119\cdot10^{-1}$
K	$1.50\cdot10^{-4}$	$1.50\cdot10^{-2}$	$1.405\cdot10^{-3}$
Mg	$4.00\cdot10^{-5}$	$4.00\cdot10^{-3}$	$5.815\cdot10^{-3}$
Ca	$1.20\cdot10^{-4}$	$1.20\cdot10^{-2}$	$1.007\cdot10^{-2}$
Sr	$1.63\cdot10^{-6}$	$1.63\cdot10^{-4}$	
F^-	$6.00\cdot10^{-5}$	$6.00\cdot10^{-3}$	
Cl^-	$4.00\cdot10^{-4}$	$4.00\cdot10^{-2}$	$4.000\cdot10^{-2}$
Br^-	$6.50\cdot10^{-6}$	$6.50\cdot10^{-4}$	
SO_4^{2-}	$4.17\cdot10^{-3}$	$4.17\cdot10^{-1}$	$9.652\cdot10^{-2}$
NO_3^-	$1.30\cdot10^{-4}$	$1.30\cdot10^{-2}$	
Alk (HCO_3^-)	$4.40\cdot10^{-3}$	$4.40\cdot10^{-1}$	$1.046\cdot10^{-3}$

*Charge balance error (%) 1.60

a very large charge unbalance (more than 45%, excess of 1.31 eq·L^{-1} of cations). In this way, the values reported by UniBern for the same type of tests with the same samples were selected for our calculations (Table 2-1). These values correspond to the concentration in water from the leachate tests where the total amount of water is 60 mL, for a solid mass of 6 g. Therefore, conversion of these values to concentration of the initial porewater in the bentonite is as follows:

$$[Species]\,(mol/L)\cdot\frac{0.06\ L}{6\ g\ dry\ clay}\cdot\frac{1\ g\ dry\ clay}{0.1\ g\ porewater}\cdot\frac{1000\ g\ porewater}{1\ L\ porewater}$$ Equation 2-1

where [Species](mol·L^{-1}) is the concentration (in mol·L^{-1}) of a given chemical species in the aqueous leachate. A water ratio (mass of porewater/mass of dry clay) of 10% is used for the calculations based on the initial water content of the bentonite /Karnland et al. 2009/. By using equation 2-1 and the values listed in column 1 in Table 2-1, the concentrations for the initial composition of the bentonite porewater have been calculated (column 2 in Table 2-1).

The concentration of some exchangeable cations like Na^+, K^+, Ca^{2+}, and Mg^{2+}, and also the concentration of SO_4^{2-}, point to the hypothesis that the porewater composition of the reference bentonite blocks was modified during the leaching test due to (1) gypsum dissolution, and (2) subsequent exchange reactions.

The partial pressure of CO_2 ($10^{-2.5}$ atm), calculated in PHREEQC for the water composition shown in column 2 in Table 2-1 is much higher than the atmospheric partial pressure ($10^{-3.5}$ atm). Since these aqueous leachates were performed in laboratory conditions, one would expect a partial pressure for CO_2 close to atmospheric conditions.

According to the processes identified that most likely have modified the composition of the original bentonite porewater during the preparation of the aqueous leachates, the composition of the initial bentonite porewater, shown in column 2 in Table 2-1, has been corrected by performing the following calculations in PHREEQC:

- C(IV) concentration in equilibrium with $P(CO_2) = 10^{-3.5}$ atm,
- S(VI) concentration in equilibrium with gypsum,
- concentration of Na^+, K^+, Ca^{2+} and Mg^{2+} in equilibrium with the composition of the cation exchange sites as reported in /Karnland et al. 2009/.

No Donnan equilibrium has been accounted for, despite this effect could be huge for such low water contents. The corrected composition of the reference water A213 is shown in column 3 in Table 2-1.

Table 2-2. Composition of the Äspö groundwater (Äspö GW, taken from borehole HG0038B01) that supplied the LOT A2 test /Karnland et al. 2009/.

Parameter	Supply water: Äspö GW (mol·L^{-1})
pH	6.9
Analytical error (%)	5.40
Ionic strength	$2.5 \cdot 10^{-1}$
Cl	$1.78 \cdot 10^{-1}$
Na	$9.60 \cdot 10^{-2}$
K	$2.60 \cdot 10^{-4}$
Ca	$5.60 \cdot 10^{-2}$
Mg	$1.60 \cdot 10^{-3}$
SO_4^{2-}	$6.00 \cdot 10^{-3}$
HCO_3^-	$4.40 \cdot 10^{-4}$
Si	$1.60 \cdot 10^{-4}$

The Äspö groundwater that supplied the LOT A2 test (by applying a constant pressure of 1.2 MPa) is the one measured at the borehole HG0038B01 (Table 2-2). It is characterized by a circum-neutral pH. At 15°C, this water sample is slightly unsaturated with calcite and calcium sulphates (gypsum and anhydrite), but it is close to equilibrium with quartz, reflecting the mineralogy of the granitic rocks at the Äspö HRL.

As for the initial porewater of bentonite, there is no available data for the redox potential of the Äspö groundwater sample. Since bentonite was prepared in laboratory and emplaced in the Äspö HRL under atmospheric conditions, the initial porewater is expected to be close to equilibrium with atmospheric O_2 ($10^{-0.68}$ atm). When bentonite is placed in the Äspö HRL (isolated from the atmospheric behaviour), the heterogeneous and homogeneous reactions evolve, exhausting the atmospheric oxygen dissolved in the porewater by the oxidation of the reductant species, mainly. In this way, pyrite equilibrium should be the redox potential controlling process. /Puigdomenech et al. 2001/ have thoroughly analysed the redox potential of groundwaters at Äspö HRL, within the REX experiment. From this work it is concluded that Äspö groundwaters are typically reducing with low to negligible dissolved oxygen concentrations.

Although there are evidences that point to very different redox conditions for the initial porewater of the bentonite blocks and the Äspö groundwater, no redox reactions have been considered in the numerical simulations performed here. The reasoning for discarding redox reactions and pyrite reactivity in the numerical simulations will be explained in more detail in Section 4.2.5.

2.1.3 Mineralogy of the bentonite blocks, copper tube and granitic host rock

The Wyoming MX-80 bentonite used in the LOT A2 test is a natural mixture of Na-montmorillonite (~ 87% by weight) and accessory minerals, among which quartz, other forms of silica and feldspars are predominant. Its mineralogy, expressed in weight percentage, is shown in Table 2-3.

This is an average initial composition that shows significant differences depending of authors and measurement techniques.

Table 2-3. Mineralogical composition of the Wyoming MX-80 bentonite, based on /SKB 2004/.

Mineral (wt%)	MX-80
Montmorillonite	87
Quartz	5
Feldspar + mica	7
Pyrite	0.07
Gypsum	0.7

The specific surface area of the bentonite grains is around $5.5 \cdot 10^5$ $m^2 \cdot kg^{-1}$ material and the grain density is around 2750 $kg \cdot m^{-3}$. Dispersed in distilled water, the clay fraction (grain size < 2 μm) makes up around 80%. The mean mineralogical composition of the montmorillonite is given by /Karnland et al. 2009/:

$$(Si_{7.92}Al_{0.08})(Al_{3.10}Fe^{3+}_{0.4}Fe^{2+}_{0.02}Mg_{0.48})O_{20}(OH)_4\ Na_{0.48}Ca_{0.04}Mg_{0.02} \qquad \text{Equation 2-2}$$

The thermodynamic stability of gypsum and anhydrite is strongly sensitive with respect to temperatures. As it has been commented previously, the temperature differences between the laboratory and the test environment are very significant (25°C and 130°C, respectively). At high temperatures, gypsum is not stable, and anhydrite is the thermodynamically favoured Ca-sulphate phase. This implies that during heating gypsum is likely transformed into anhydrite. These two phases have a different thermodynamic and kinetic behaviour, being gypsum dissolution a faster process than anhydrite dissolution. This can result in a mismatch between the total amount of Ca-sulphate analyzed in the samples and the amount of reactive Ca-sulphate present in each section of bentonite after the heater is switched on. As it will be shown later, the numerical results are very sensitive with respect to the amount of initial gypsum-anhydrite. Therefore, despite the total amount of Ca-sulphate is given by the analysis of reference samples, sensitivity analyses have been performed.

The cation exchange capacity is around 0.75 $eq \cdot kg^{-1}$ bulk material and around 0.85 $eq \cdot kg^{-1}$ clay fraction. The natural exchangeable cations and their occupancies are:

- Na^+ (~70%),
- Ca^{2+} (~20%),
- Mg^{2+} (~ 6%) and,
- K^+ (~2%).

The copper tube is composed of pure oxygen-free copper and, according to the results of the LOT A2 test, some copper can be incorporated in the bentonite matrix in the first 2 cm of the bentonite blocks around the copper tube.

The granitic rock at Äspö is composed of granodiorite to quartz-monzodiorite rocks, and the main minerals present are quartz, plagioclase, K-feldspar and mica /Wahlgren et al. 2008/.

2.1.4 Physical properties of the bentonite blocks

In order to produce the bentonite rings that have been placed between the copper canister and the granitic host hock, the bentonite was compacted without pre-treatment. Compaction of bentonite blocks was performed in a uniaxial compaction device that was specially designed to produce bentonite blocks with accurate dimensions, density and composition /Karnland et al. 2009/.

The initial degree of water saturation of the compacted bentonite blocks was calculated from the initial water content of different reference samples /Karnland et al. 2000/, and from a mass balance calculation performed for chloride which is considered to behave conservatively, as its mobility is mainly influenced by the water flow and its interaction with the solid phase is negligible. In this context, the chloride concentration in the porewater of the bentonite blocks at the end of the LOT A2 test should represent the pure mixture between the initial bentonite porewater and the Äspö groundwater that was used to hydrate the initially partially saturated bentonite blocks.

The chloride profile for blocks located close to the heater, at the end of the 6 years of the LOT A2 test, is shown in Figure 2-3. At the end of the experiment, the chloride is almost homogeneously distributed along the radial distance of the three bentonite blocks analysed (blocks A209BSb, A211BWb and A233BWb, Figure 2-2b).

From the data plotted in Figure 2-3, the average chloride concentration in A209BSb, A211BWb and A233BWb is $1.1 \cdot 10^{-1}$ $mol \cdot L^{-1}$. If we consider that this final concentration is a pure mixture of chloride from the initial bentonite porewater and chloride from the Äspö groundwater, and knowing

that at the end of the experiment the bentonite is fully water saturated, we may calculate the initial degree of saturation (S_r) by using the following equation:

$$S_r = \frac{[Cl^-]_{Final} - [Cl^-]_{Äspö}}{[Cl^-]_{Initial} - [Cl^-]_{Äspö}} \qquad \text{Equation 2-3}$$

where $[Cl^-]_{Äspö}$ is the concentration of chloride in Äspö groundwater (Table 2-2), $[Cl^-]_{Final}$ is the concentration of chloride at the end of the experiment, and $[Cl^-]_{Initial}$ is the concentration of chloride in the initial bentonite porewater ($4.0 \cdot 10^{-2}$ mol·L^{-1}, Table 2-1).

Table 2-4. Measured chloride concentration at the end of the LOT A2 test in blocks A209BSb and A211BWb, in the reference sample (A213), and in the Äspö groundwater that supplied the LOT A2 test /Karnland et al. 2009/. Degree of saturation calculated according to equation 2-2 for each measuring point and average value calculated using all measuring points considered.

Sample reference	Distance from Cu tube (cm)	[Cl$^-$] (mol·L^{-1})	Initial degree of saturation (unitless)	Average of the initial degree of saturation (unitless)
A2 09	1	$1.08 \cdot 10^{-1}$	0.51	0.51
A2 09	3	$1.04 \cdot 10^{-1}$	0.53	
A2 09	5	$1.04 \cdot 10^{-1}$	0.53	
A2 09	7	$1.06 \cdot 10^{-1}$	0.52	
A2 09	9	$1.14 \cdot 10^{-1}$	0.46	
A2 11	1	$1.01 \cdot 10^{-1}$	0.56	
A2 11	3	$1.05 \cdot 10^{-1}$	0.53	
A2 11	5	$1.03 \cdot 10^{-1}$	0.54	
A2 11	7	$1.15 \cdot 10^{-1}$	0.46	
A2 11	9	$1.19 \cdot 10^{-1}$	0.42	
A2-13-1		$4.00 \cdot 10^{-2}$		
Äspö GW		$1.78 \cdot 10^{-1}$		

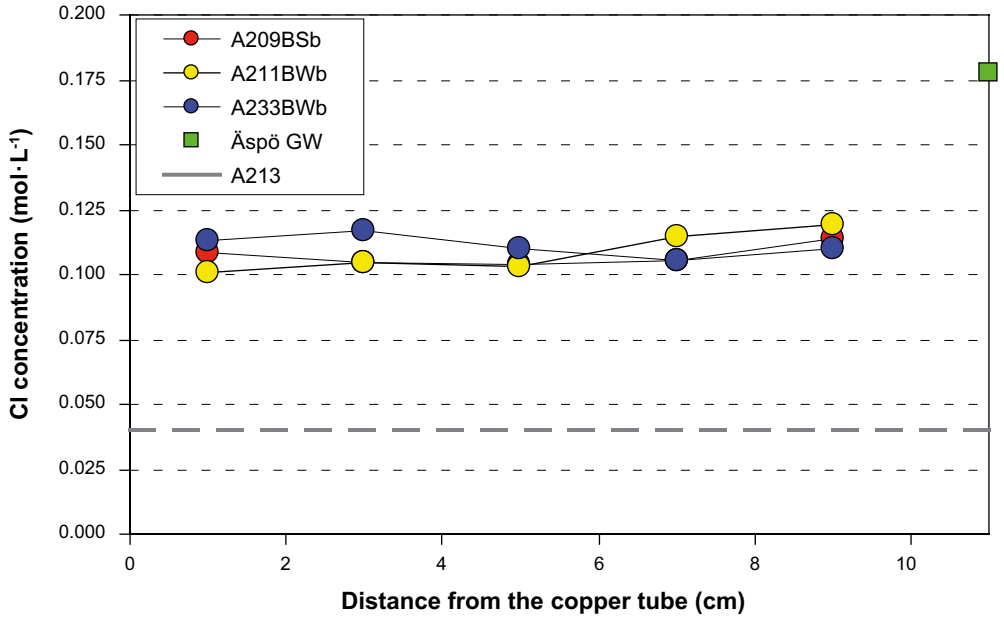

Figure 2-3. *Radial profile of chloride concentration measured after the 6 years test, in the blocks A209BSb, A211BWb and A233BWb of the LOT A2 test. The chloride concentration in the reference bentonite porewater (A213) and in Äspö groundwater (Äspö GW) are also shown.*

The degree of saturation has been calculated for each data point (Table 2-4). The averaged initial degree of saturation is 50%. Other estimations performed from the water content /Karnland et al. 2000/ are consistent with this approximation.

According to the results of the LOT A2 test, the hydraulic conductivity of the compacted bentonite blocks is a function of the corresponding saturated density /Karnland et al. 2009/ which has an average value of 2.00 kg·dm^{-3}. By using this value and the relation between saturated density and hydraulic conductivity shown in Figure 2-4, under fully water saturated conditions, a hydraulic conductivity around $1\cdot10^{-13}$ m·s^{-1} is obtained. It corresponds to an absolute permeability of $1\cdot10^{-20}$ m^2, by assuming a water density of 1000 g·m^{-3}, a dynamic water viscosity of $1\cdot10^{-3}$ N·s·m^{-2}, and using the following equation:

$$K = k_r k \cdot \frac{\rho_w g}{\mu_w}$$ Equation 2-4

where K is the hydraulic conductivity in m^2·s^{-1}; k_r is the relative permeability fraction (unitless; 1 for fully water saturated media); k is the absolute permeability in m^2; ρ_w is water density in g·m^{-3}; g is the gravitational acceleration (9.8 m^2·s^{-1}).

In Table 2-5, the average values for the physical and hydraulic parameters of the reference bentonite blocks that have been measured within the LOT A2 Project are listed.

Table 2-5. Physical properties of the reference bentonite blocks that were placed in the LOT A2 test between the copper tube and the granitic host rock /Karnland et al. 2009/.

Parameter	Units	Symbol	Average Value
Grain density	kg·m^{-3}	ρ_s	2750
Saturated density	kg·m^{-3}	ρ_{sat}	2000
Dry density	kg·m^{-3}	ρ_d	1570
Porosity	unitless	ϕ	0.43
Effective diffusion coefficient	m^2·s^{-1}	D_e	$5\cdot10^{-14}$ – $1\cdot10^{-9}$
Absolute permeability	m^2	k	$1\cdot10^{-20}$
Initial degree of saturation	unitless	S	0.48–0.50 [(a)]

[(a)] Calculated from (1) the chloride mass balance and (2) the initial water content.

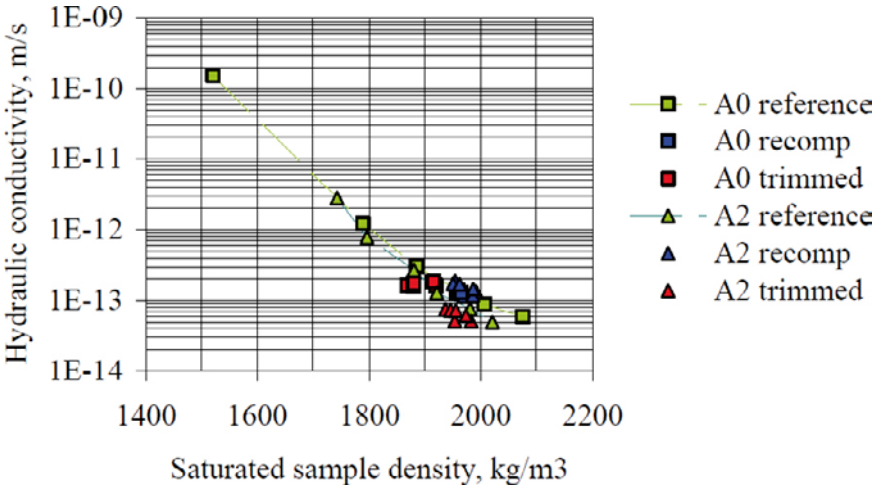

Figure 2-4. *Measured hydraulic conductivity from the A2 parcel material compared with results from the reference material and to the previous one year test material (A0) (reproduced with permission from /Karnland et al. 2009/).*

3 Description of the conceptual model

The numerical model developed here is intended to reproduce the water saturation, the transport of solutes and the geochemical reactions that occurred in the bentonite blocks A209BSb and A211BWb of the LOT A2 test, located at the depth of the heater where the highest thermal gradient was established. An additional case at a constant temperature of 25°C, representing the block A233BWb in the upper non-heated part of the parcel, has been simulated for comparison.

3.1 Flow of water, gas and heat in the bentonite

The LOT A2 test parcel has been developed to assess the process of bentonite saturation and the geochemical reactions occurring under the hydro-thermo-mechanical conditions expected around the HLNW containing canisters of a KBS-3 repository, but with a higher maximum temperature than that expected in the repository and a different thermal gradient (as a consequence of the maximum temperature and the smaller dimensions of the experiment). This means that the LOT A2 test has been developed under more adverse thermal conditions than those expected in a KBS-3 repository; a temperature of 130°C was induced at the surface of the copper tube of the LOT A2 test, instead of the 90°C that are expected in a KBS-3 repository. As a consequence of the "scale effect" of the experiment, the time scale for saturation is also modified.

In a KBS-3 repository the bentonite is placed between the copper canister and the host rock. At the inner border of the bentonite rings, the copper canister transfers heat (due to the radioactive decay of the HLNW) to the surrounding bentonite, and at the outer border of the bentonite rings the saturated host rock induces a hydraulic (and also mechanical) pressure over the bentonite (Figure 3-1). Heat transport occurs by convection (advection), and conduction (diffusion), while water flow is induced by pressure gradients and capillary forces.

Under the conditions of a KBS-3 repository, as soon as the bentonite comes into contact with groundwater the process of saturation begins. During this process the swelling of the clay minerals results in the redistribution of the pore space leading to changes in the bentonite permeability. When the bentonite becomes fully water saturated, it is expected that the mobile water moves very slowly due to the low permeability /Kröhn 2003/.

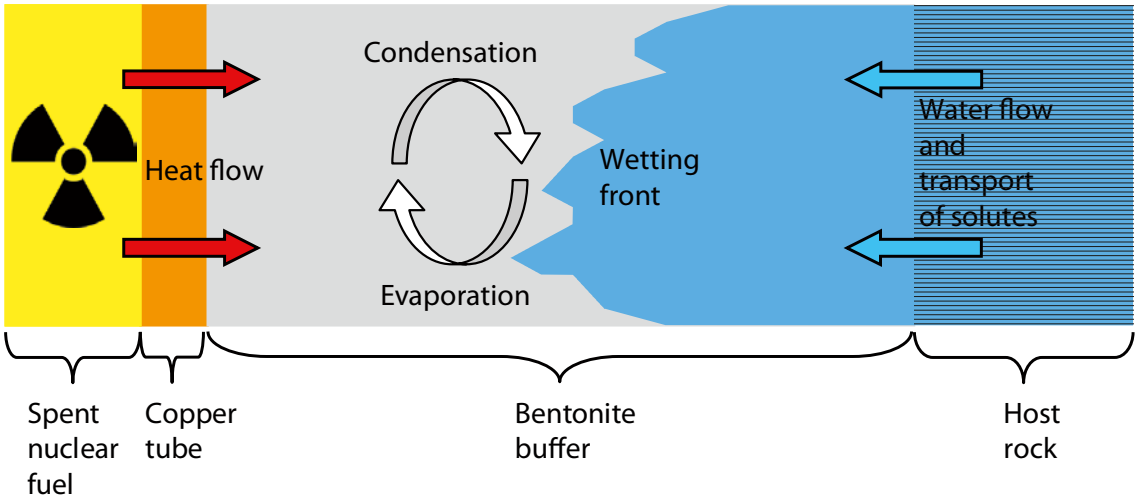

Figure 3-1. *Sketch of a vertical cross section of the near-field of a KBS-3 repository showing the thermo-hydraulic and transport processes that are believed to occur during the saturation period of the bentonite buffer.*

Besides the aqueous phase, the gaseous phase is also expected to move through the bentonite pores due to (1) the process of saturation that pushes the air towards the copper tube, and (2) to evaporation of water close to the heater. Gas flow in porous media differs from liquid flow due to the combined effect of the large compressibility of gas, and the Klinkenberg effect /Wu et al. 1998/, which have a significant impact on gas flow. These phenomena are especially relevant in low permeability media such as in the compacted bentonite modelled here. The Klinkenberg effect is due to the slip flow of gas at pore walls which enhances gas flow when pore sizes are very small, and its effect explains (1) the much higher gas permeability compared to that of water and (2) the enhancement of gas permeability with increasing pore pressure /Tanikawa and Shimamoto 2006/.

3.2 Transport and reactivity of solutes in the bentonite

The thermal gradient induced by the heater and the gradual saturation of the bentonite buffer that progresses from the contact with the host rock towards the copper tube are expected to trigger the following processes /Karnland et al. 2009/:

1) Ion transport parallel to water uptake from the outer cooler parts of the bentonite, or from the surrounding groundwater, to the wetting front in the originally unsaturated bentonite (Figure 3-1). The transport is assumed to take place by a cyclic evaporation/condensation process in which water is sucked in from the cooler parts and evaporates at the wetting front (Figure 3-1).
2) Precipitation/dissolution of solids, such as anhydrite, calcite and silica, and cation exchange reactions. These processes may take place both in the unsaturated and fully saturated bentonite.

3.2.1 Transport processes

During the period of saturation of the bentonite buffer, a piston-like water flow is expected to occur, i.e. as Äspö groundwater fills the partially saturated bentonite pores, the initial porewater is pushed by the inflowing Äspö groundwater towards the copper tube. During the saturation period, besides the cyclic evaporation/condensation process close to the heater, advection should play an important role on the transport of solutes.

When the bentonite is fully water saturated, the transport of solutes is manly controlled by diffusion which tends to homogenize the distribution of solutes in the bentonite pores, as already seen for the case of chloride (Figure 2-3). Besides diffusion, and depending on the type of solute, other processes such as geochemical reactions can influence solute mobility. Chloride transport, for instance, can be markedly influenced by Donnan equilibrium or osmosis /Birgersson and Karnland 2009/; /Muurinen et al. 2004/.

Data included in previous works on the diffusion coefficients of bentonite are related to laboratory environmental conditions (around 10^{-10} – 10^{-11} $m^2 \cdot s^{-1}$ /Arcos et al. 2003/). This is typical for the actual diffusivity in the clay.

It is well-known that the diffusion coefficient in water (D_{aq}) depends on temperature, both directly and through the effect of temperature (T) on the solution viscosity (μ). Since in two of the LOT A2 modelled blocks (A209BSb and A211BWb) the bentonite reached a temperature ranging from 130 to 85°C, the diffusion coefficients that will be implemented in the numerical models of these cases must be substantially higher than those reported for laboratory conditions. For low temperatures, the temperature dependence of aqueous diffusion coefficients can be calculated through the relationship $D_{aq}\mu/T$ = constant. Also, an approximate dependence of the diffusion coefficient on temperature in liquids can be found using the Stokes-Einstein equation that shows an increase in the coefficient as a function of the increment of temperature and the dynamic viscosity of the liquid (which is strongly thermal dependent). In this context, some authors have proposed an increase around two orders of magnitude in heated water environments (related to the typical values at 25°C; /Lerman 1971, Schwartz and Zhang 2003/). This is in accordance with the diffusion coefficient implemented in the analytical evaluation of the THM modelling exercise of the buffer, backfill and other system components ($1.4 \cdot 10^{-8}$ $m^2 \cdot s^{-1}$; /Åkesson et al. 2010/).

3.2.2 Geochemical processes

The most important mineral in the MX-80 bentonite used in the LOT A2 test is montmorillonite (~87 wt%; Table 2-3). Therefore, one of the most significant geochemical processes expected to influence solute mobility in the bentonite is the cation exchange in the montmorillonite interlayer.

Taking into account the concentration of sulphate, bicarbonate and calcium ions in the initial porewater of bentonite and Äspö groundwater (Table 2-2), combined with the high temperature under which the LOT A2 test was developed, the most important solid phases that will be involved in the precipitation/dissolution processes are calcite and anhydrite. In fact, the results of preliminary static geochemical calculations performed with PHREEQC /Parkhurst and Appelo 1999/ indicate that, at 15°C (which is the average temperature of Äspö groundwater at 450 m depth), the Äspö groundwater is slightly unsaturated with respect to calcite ($SI_{calcite} = –0.54$), while at 130°C it becomes oversaturated ($SI_{calcite} = 0.44$). The calculated bentonite porewater at 15°C was forced to be in equilibrium with gypsum and it is slightly unsaturated with respect to calcite ($SI_{calcite} = –0.13$), while at 130°C it becomes oversaturated with respect to calcite ($SI_{calcite} = 0.47$), and approaches the equilibrium with anhydrite ($SI_{anhydrite} = –0.20$), it is worth noting that above around 56°C, gypsum is not stable anymore, being anhydrite the thermodynamically favoured calcium sulphate phase.

It should be noted that, besides the temperature effect, the evaporation of the bentonite porewater induced by the thermal gradient, should lead to the increase of the concentration of solutes close to the copper canister which in turn could favour the precipitation of the abovementioned mineral phases: calcite and anhydrite.

According to /Karnland et al. 2009/, at the end of the LOT A2 test, sulphate minerals were distributed along the thermal gradient in the heated blocks; anhydrite accumulated approximately 3-5 cm from the copper canister, whereas the rest was depleted in sulphates. On the contrary, in the non-heated bentonite, the distribution of sulphate minerals seems to be non-affected or very slightly depleted. In the heated blocks, the content on carbonate minerals decreased with increasing temperature.

The precipitation/dissolution of Ca-sulphates and carbonates during the LOT A2 test influenced the composition of the bentonite porewater which, in turn, triggered the replacement of exchangeable Na^+ by Ca^{2+}, in the inner parts of the heated blocks /Karnland et al. 2009/. The geochemical profiles of the bentonite rings at the end of the LOT A2 test also show that exchangeable Mg^{2+} increases with increasing temperature in the heated blocks /Karnland et al. 2009/.

From the solutes present in the two waters used in the LOT A2 test (Table 2-1 and Table 2-2), and taking into account the information provided in the previous paragraphs, the solutes expected to be markedly influenced by heterogeneous (solid-aqueous) geochemical reactions are Na^+, K^+, Ca^{2+}, Mg^{2+}, SO_4^{2-} and HCO_3^-.

As previously explained (Section 2.1.2), due to their relatively small impact during the process of bentonite saturation /Arcos et al. 2003, 2006/, redox processes and also the dissolution of sulphide minerals that are present in the bentonite mineralogy will not be considered in the numerical simulations.

Although there are evidences of the incorporation of a small fraction (~0.5%) of copper in the bentonite matrix that contacts the copper tube /Karnland et al. 2009/, the transfer of copper from the copper tube to the bentonite matrix has been discarded from the numerical simulations performed here, because this geochemical process is very local (it is observed only in the first 2 cm of the bentonite, from the copper tube) and has a relatively low impact on the behaviour of major elements geochemistry of the bentonite blocks.

3.3 THMC experiment with FEBEX bentonite

In order to improve our understanding of the process occurring during bentonite saturation and the associated transport of conservative solutes, it was decided to build a numerical model of an experiment conducted by CIEMAT with the FEBEX bentonite /Villar et al. 2006/, which is a smaller scale experiment than the LOT A2 test. In addition, while in the LOT A2 test experimental data are only available for the initial and final stages, in the laboratory experiment with FEBEX bentonite (hereafter called FEBEX experiment), data at different time intervals are available and, therefore, provide an additional instrument to test and validate our conceptual model.

3.3.1 Setup of the numerical model developed for the FEBEX experiment

The FEBEX experiment modelled here consists of a 60 cm-long by 7 cm-diameter column of compacted bentonite extracted from the Cortijo de Archidona deposit (SE Spain). The compacted bentonite blocks used in the FEBEX experiment were manufactured by uniaxial compaction of the granulated clay with a dry density of 1.42 kg·dm^{-3}, and a gravimetric water content of 33.7% when fully water saturated /Villar et al. 2008a/. According to these experimental data, the estimated porosity(ϕ) is:

$$\phi = \frac{0.337 kg\_of\_water}{1 kg\_of\_bentonite} \times \frac{1 L\_of\_water}{1 kg\_of\_water} \times \frac{1.42 kg bentonite}{1 L bentonite} \times \frac{1 L\_of\_porosity}{1 L\_of\_water} = 0.48$$

Equation 3-1

which is in the range of the values reported in /Villar et al. 2008a/ (0.43 to 0.50).

Knowing that the gravimetric water content of the compacted bentonite blocks placed in the column is 13.7% /Villar et al. 2008b/, and using the above calculated porosity of 0.48, the initial water saturation degree of the compacted bentonite (S_r) is:

$$S_r = \frac{0.137 kg\_of\_water}{1 kg\_of\_bentonite} \times \frac{1 L\_of\_water}{1 kg\_of\_water} \times \frac{1.42 kg bentonite}{1 L bentonite} \times \frac{1 L\_of\_bentonite}{0.48 L\_of\_porosity} = 0.41$$

Equation 3-2

According to /Villar et al. 2008a/, the absolute permeability of the compacted bentonite used in the FEBEX experiment is $1.41 \cdot 10^{-20}$ m^2. Since there are no reported values for the diffusion coefficient of the bentonite used in the FEBEX experiment, the value of this parameter has been estimated through calibration of the numerical model and based on the values reported for the LOT A2 test. The calibrated effective diffusion coefficient is $1.0 \cdot 10^{-11}$ m^2·s^{-1}.

According to the description of the FEBEX experiment /Villar et al. 2007/, the bentonite column can be interpreted as a 1D numerical problem with the geometry and boundary conditions as shown in Figure 3-2.

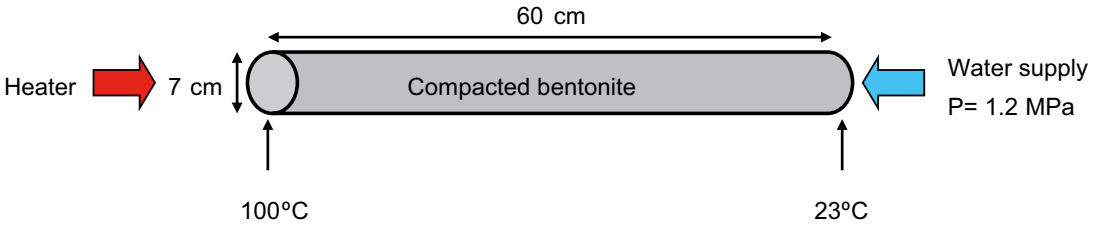

Figure 3-2. *Sketch of the 1D numerical model developed to simulate the FEBEX experiment.*

TOUGHREACT /Xu et al. 2008/ is the reactive transport numerical code used in this work (see Section 4.1). In the numerical model that simulates the FEBEX experiment, the functions leading to the best agreement between measured and simulated water saturation profile are:

- for the relative permeability: both phases (liquid and gas) have been modelled as perfectly mobile,
- for the capillary pressure: Leverett's function has been used (see Section 4.2.3).

Although /Villar et al. 2008b/ applied the Van Genuchten equation for the capillary pressure function to simulate the evolution of water saturation in the FEBEX experiment by using the numerical code CODE-BRIGHT /Olivella et al. 1996/, we have attained better results with the Leverett's function using the numerical code TOUGHREACT (see Section 4.2.3). These results reflect the relatively high degree of uncertainty related to the capillary pressure function that is most suitable in highly non-linear problems such as the saturation of bentonite under non-isothermal conditions. The parameters to which we have to assign the characteristic values are the characteristic capillary pressure (P_0), and the irreducible water content (S_{lr}). After calibration, we have obtained a P_0 of $2.2 \cdot 10^{-2}$ MPa and a S_{lr} of 0.0 for the compacted bentonite of the FEBEX experiment.

For the Klinkenberg effect (see Section 4.2.3; equation 4-13), we have obtained a calibrated value for the parameter b of 10 MPa.

The values of the hydraulic parameters used in the numerical model of the FEBEX experiment are summarised in Table 3-1.

The porewater composition of the bentonite used in the FEBEX experiment, measured in mmol of solute per 100 g of bentonite, has been converted to $mol \cdot L^{-1}$ (which is the unit for solute concentration in TOUGHREACT) by using the following equation:

$$[solute]_{mol/L} = \frac{[solute]_{mmol/100g\_of\_bentonite}}{100g\_of\_bentonite} \times \frac{1mol}{1000mmol} \times \frac{\rho_{dry}}{\phi \times S_r} \qquad \text{Equation 3-3}$$

where ρ_{dry} is the dry density of bentonite (1.42 $kg \cdot L^{-1}$), ϕ is the porosity of bentonite (0.48) and S_r is the initial water saturation degree of bentonite (0.41).

Table 3-1. Summary of the hydraulic data used in the numerical model of the FEBEX experiment.

Parameter	Symbol	Value	Units
Porosity	ϕ	0.48	Unitless
Absolute permeability	k	$1.41 \cdot 10^{-20}$	m^2
Effective diffusion coefficient	D_e	$1.00 \cdot 10^{-11}$	$m^2 \cdot s^{-1}$
Characteristic capillary pressure	P_0	$2.20 \cdot 10^{-2}$	MPa
Irreducible water saturation	S_{lr}	0.0	Unitless
Klinkenberg parameter	b	10	MPa

Table 3-2. Composition of the initial porewater of the bentonite and supplying water used in the FEBEX experiment.

Parameter	Initial bentonite porewater		Water supplied
	mmol/100g of bent.	$mol \cdot L^{-1}$	$mol \cdot L^{-1}$
pH	8.73		8.3
Cl	1.98	$1.43 \cdot 10^{-1}$	$3.70 \cdot 10^{-4}$
SO_4^{2-}	$9.79 \cdot 10^{-1}$	$7.09 \cdot 10^{-2}$	$1.50 \cdot 10^{-4}$
HCO_3^-	1.18	$8.58 \cdot 10^{-2}$	$2.36 \cdot 10^{-3}$
Na	5.02	$3.64 \cdot 10^{-1}$	$4.80 \cdot 10^{-4}$
K	$7.30 \cdot 10^{-2}$	$5.29 \cdot 10^{-3}$	$2.60 \cdot 10^{-5}$
Mg	$5.50 \cdot 10^{-2}$	$3.99 \cdot 10^{-3}$	$3.90 \cdot 10^{-4}$
Ca	$5.00 \cdot 10^{-2}$	$3.62 \cdot 10^{-3}$	$1.12 \cdot 10^{-3}$

A series of uncertainties related to the conceptual model (and the analytical data) have been evaluated in order to interpret the numerical results:

1. Units for solutes concentration. /Villar et al. 2006/ reported a deformation of the compacted bentonite after the experiment which is related to swelling of the bentonite and subsequent modification of the dry density of the bentonite. This alteration of the dry density of bentonite has an important impact on the chloride concentration expressed in mmol/100 g of bentonite.
2. Water content data. Experimental data for the water content of bentonite are given in kg of water/kg of bentonite. In order to convert this unit to saturation degree (volume of water/volume of porosity which is the input and output data of the numerical model), the dry density of bentonite and the corresponding porosity must be employed. These two parameters are affected by the swelling of bentonite, and therefore, uncertainties are involved in the treatment of the water content data.
3. Heterogeneity of bentonite. We assumed a homogeneous bentonite along the whole column and throughout the time span of the experiment. Nevertheless, /Villar et al. 2006/ noticed that swelling of the bentonite was more visible in the area closer to the hydration border. This means the initially homogeneous bentonite became progressively heterogeneous during the experiment.
4. As for the other hydraulic parameters, the diffusion coefficient has been assumed homogeneous in the whole column. Nevertheless, it is known that the diffusion coefficient increases with increasing temperature /Suzuki et al. 2004/.

3.3.2 Numerical results for the FEBEX experiment

With the conceptual model proposed previously, the experimental data collected during the FEBEX experiment has been successfully reproduced.

The simulated evolution of the water saturation and the thermal gradient in the FEBEX experiment are shown in Figure 3-3 and Figure 3-4, respectively. It is seen that the water saturation computed for 7.59 years of experiment agrees well with measured data. The same is true for temperature after 2 years of experiment. Finally, evaporation of the bentonite porewater close to the heater leads to a decrease of the water saturation, from an initial value of 41%, to near 20%.

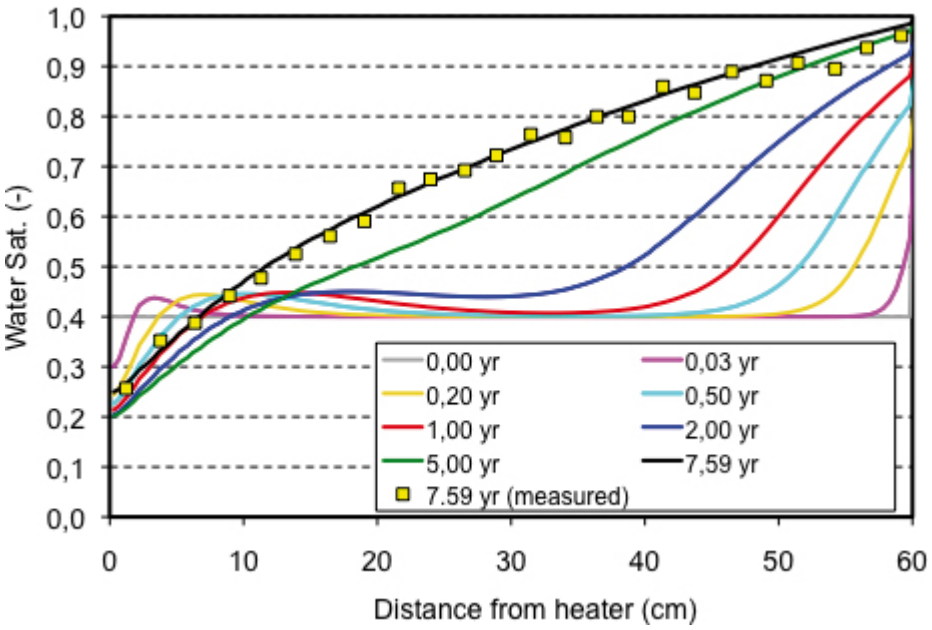

Figure 3-3. *Simulated evolution of the water saturation for the FEBEX experiment. Water saturation measured at the end of the experiment is also shown.*

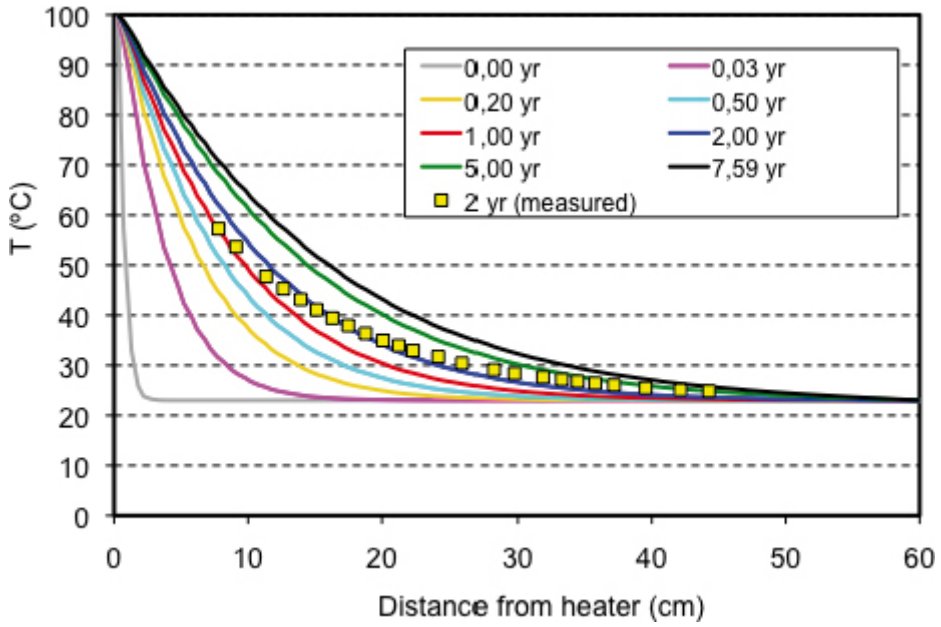

Figure 3-4. *Simulated evolution of the thermal gradient for the FEBEX experiment. The temperature measured in the second year of the experiment is also shown.*

The evaporation of the bentonite porewater close to the heater leads to an increase of solutes concentration. In the adjacent area, where the evaporated water condenses, the observed effect is dilution. Although there is an increase of the concentration of solutes in the area affected by evaporation, chloride salts do not reach oversaturation, and therefore chloride can be treated as a conservative solute.

The numerical results computed for the transport of chloride agree relatively well with measured data (Figure 3-5, Figure 3-6). Although there are some discrepancies, the overall tendencies of measured chloride are reproduced by the numerical model which validates our conceptual model.

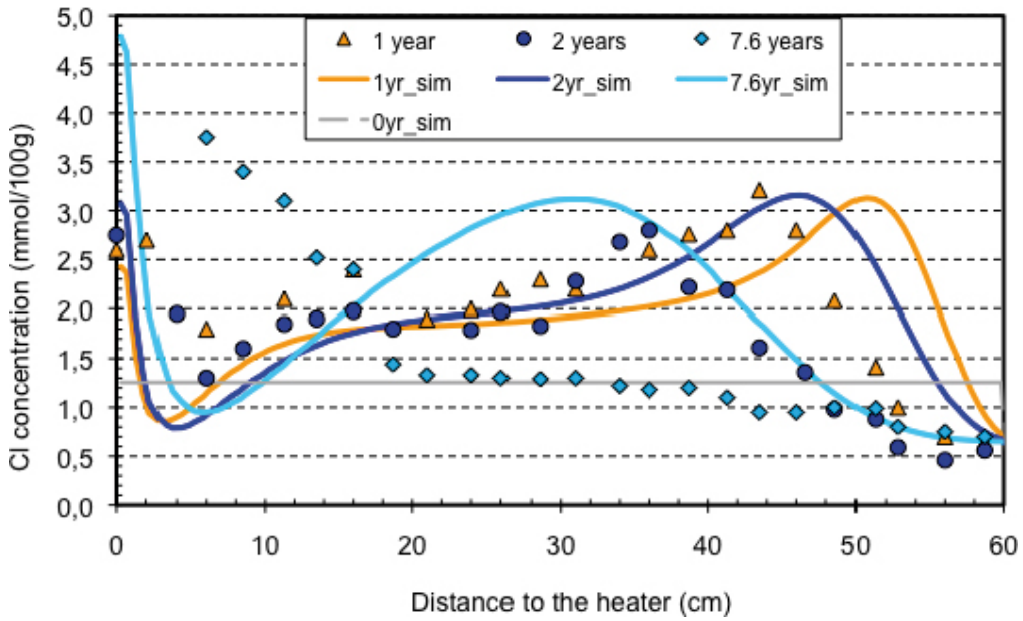

Figure 3-5. *Measured and simulated data for the chloride profiles in the compacted bentonite column of the FEBEX experiment. Case where simulated water saturation agrees with measured data.*

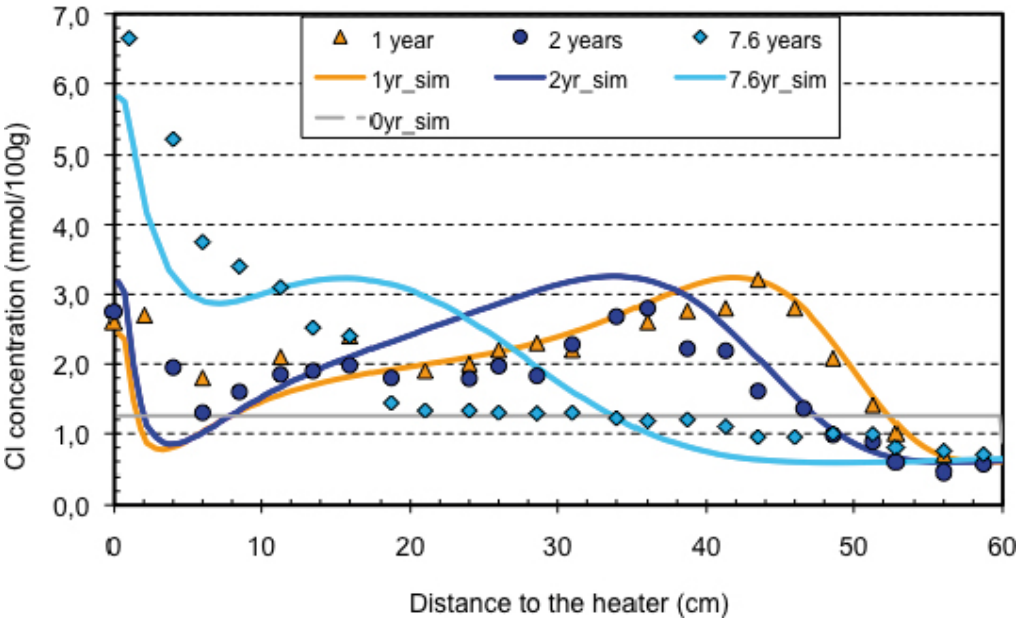

Figure 3-6. *Measured and simulated data for the chloride profiles in the compacted bentonite column of the FEBEX experiment. Case where simulated water saturation overestimates measured data (P0 $8 \cdot 10^{-2}$ MPa instead of $2.2 \cdot 10^{-2}$ MPa.*

The chloride concentration peaks observed close to the heater are due to the combined effect of evaporation and suction of bentonite porewater from the area adjacent to the heated border. On the other hand, the peaks of chloride concentration observed for 1 and 2 years of experiment close to the hydration border, propagate in the direction of bentonite saturation, reflecting the piston-like phenomena that prevails during bentonite saturation. In other words, during bentonite saturation, the water injected in the bentonite column, which has a lower chloride concentration than the bentonite porewater, pushes the former bentonite porewater towards the heater, leading to peaks of chloride concentration at 42 cm and 36 cm after after 1 and 2 years respectively.

As shown in Figure 3-5, the simulated chloride peaks for 1 and 2 years, located at 52 and 46 cm respectively, are delayed with respect to measured data. In order to understand the reason for this discrepancy, we performed an additional simulation by calibrating the Leverett's capillary function in such a way that these chloride peaks agree better with measured data (Figure 3-6). Nevertheless, in this alternative model, computed water saturation for the bentonite column overestimates measured data; i.e. the numerical results lead to an almost fully water saturated bentonite column at the end of the experiment.

These differences between the analytical data and the results are more significant at more advanced calculation times. Therefore, this disagreement is a clear indication that the physico-chemical properties of the bentonite changes along the experiment. This evolution in the bentonite properties (see Section 3.3.1) has not been implemented in the numerical model as it is beyond the scope of the present work.

We can conclude that the qualitative agreement obtained between analytical and computed data, besides the differences due to the abovementioned uncertainties, supports the application of the conceptual model to the case of the LOT A2 test.

4 Numerical model setup

4.1 Numerical tool and thermodynamic database

The numerical tool used in the calculations is the code TOUGHREACT /Xu et al. 2008/. This code results from coupling the calculation of geochemical reactions to the THOUGH2 code /Pruess et al. 1999/, which solves multiphase, non-isothermal fluid flow, heat flow and multi-component transport. TOUGHREACT accommodates chemical species present in liquid, gas and solid phases. Aqueous complexation, gas dissolution/ex-solution, and cation exchange are modelled under local equilibrium. On the other hand, mineral precipitation/dissolution may be modelled either under equilibrium or kinetics assumptions. Additionally, changes in porosity, permeability, and capillary pressure, owing to mineral precipitation/dissolution, may be computed /Pruess et al. 1999/.

The major assumptions considered in TOUGH2 for the simulation of non-isothermal fluid and heat flows are /Xu and Pruess 2001/:

1. fluid flow, in both liquid and gas phases, occurs under pressure, viscous and gravity forces,
2. interaction between flowing phases (gas and liquid) depends on characteristic curves (relative permeability and capillary pressure) and,
3. heat flow occurs by conduction, convection and diffusion.

TOUGHREACT encompasses two important phenomena: (1) gas phase is active for multiphase flow, mass transport and chemical reactions, and (2) the effects of heat include heat-driven fluid flow and temperature-dependant thermodynamic physical and geochemical properties, such as fluid density and viscosity, and thermodynamic and kinetic data for geochemical reactions. Advection and diffusion processes are considered for both the liquid and gas phases, and their coefficients are assumed to be the same for all species /Xu and Pruess 2001/.

Hydrodynamic dispersion is an important solute transport phenomenon that arises from a interplay between non-uniform advection and molecular diffusion, due to heterogeneities on multiple scales. In many numerical models, hydrodynamic dispersion is often represented by a Fickian diffusion analogue also known as the convection-dispersion equation, but not in TOUGHREACT. In this code, hydrodynamic dispersion is modelled through an appropriate spatial resolution on multiple scales, using multiple continua models to describe interactions between fluid regions with different velocities /Xu and Pruess 2001, and references therein/.

The activity coefficients of aqueous species are calculated from the Debye-Hückel equation. The activities of pure mineral phases and H_2O are assumed to be one, and gases are assumed ideal at atmospheric conditions. At higher temperatures and pressures such as boiling conditions, the fugacity coefficients of gases depend on the temperature and pressure of the system /Xu and Pruess 2001, and references therein/.

In THOUGH2, space discretization is made directly from the integral form of the basic conservation equations without converting them into partial differential equations. This method is called the integral finite difference /Pruess et al. 1999, and references therein/, and is applicable to regular or irregular space discretization in one, two, and three dimensions. Time is fully implicitly discretized as a first-order backward finite difference, while flux is 100% upstream weighted. The coupling between fluid flow, mass transport and geochemical reactions is made using a sequential iterative approach.

The mass and energy balance equations solved by TOUGH2 /Pruess et al. 1999/ may be written as follows:

$$\frac{d}{dt}\int_{V_n} M^k dV_n = \int_{\Gamma_n} F^k \cdot n d\Gamma_n + \int_{V_n} q^k dV_n \qquad \text{Equation 4-1}$$

where t is time, V_n is a volumetric grid block of the modelled domain which is bounded by the closed surface Γ_n, M represents mass or energy per volume, k labels the mass components water, air,

gases, solutes, and heat, F denotes mass or heat flux, q denotes sinks and sources for mass or energy (the sinks/ sources for mass of reactive solutes are the output of the geochemical calculations), and n is a normal vector on the surface $d\Gamma_n$, pointing inward into V_n.

The advective mass flux is a sum over phases:

$$F_{adv}^{k} = \sum_{\beta} X_{\beta}^{k} F_{\beta} \qquad \text{Equation 4-2}$$

where F_β is the flux of phase β (can be water or air), and X_β^k is the mass fraction of k in phase β. Phase fluxes (of water or air) are given by a multiphase version of Darcy's law:

$$u_{\beta} = -k\frac{k_{r\beta}\rho_{\beta}}{\mu_{\beta}}\left(\nabla P_{\beta} - \rho_{\beta} g\right) \qquad \text{Equation 4-3}$$

where u_β is Darcy's velocity or specific flow, k is absolute permeability, $k_{r\beta}$ is relative permeability to phase β, ρ_β is the density of phase β, μ_β is the viscosity of phase β, ∇P_β is the pressure gradient of phase β, and g is the gravitational acceleration.

The mass flux due to the combined effect of diffusion and hydrodynamic dispersion is as follows /de Marsily 1986, in Pruess et al. 1999/:

$$F_{dis}^{k} = -\sum_{\beta} \rho_{\beta} D_{\beta}^{k} \nabla X_{\beta}^{k} \qquad \text{Equation 4-4}$$

where ∇X_β^k is the gradient of mass fraction of component k in phase β, and D_β^k is the hydrodynamic dispersion tensor which is related to the transverse and longitudinal dispersion coefficients and these, in turn, are given by the following equations which relate the dispersion coefficient to tortuosity:

$$D_{\beta,L}^{k} = \phi\tau_0\tau_{\beta} d_{\beta}^{k} + \alpha_{\beta,L} u_{\beta} \qquad \text{Equation 4-5}$$

$$D_{\beta,T}^{k} = \phi\tau_0\tau_{\beta} d_{\beta}^{k} + \alpha_{\beta,T} u_{\beta} \qquad \text{Equation 4-6}$$

where $D_{\beta,L}^k$ and $D_{\beta,T}^k$ are the longitudinal and transverse dispersion coefficients, respectively, ϕ is porosity, $\tau_0\tau_\beta$ is the tortuosity which includes a porous medium dependant factor (τ_0) and a coefficient that depends on phase saturation (τ_β), d^k_β is the molecular diffusion coefficient, and $\alpha_{\beta,L}$ and $\alpha_{\beta,T}$ are the longitudinal and transverse dispersivities, respectively.

Finally, the effective diffusion coefficient (D^k_e) is related to the tortuosity (τ) and the molecular diffusion coefficient (d^k_β), according to the following equation:

$$D_{e}^{k} = \tau d_{\beta}^{k} \phi \qquad \text{Equation 4-7}$$

The thermodynamic database used in TOUGHREACT is the EQ3/6 database, developed by /Worely 1992/ which is commonly used in geochemical models. The thermodynamic database includes reaction stoichiometries, dissociation constants (log(K)), and regression coefficients of log(K) as a function of temperature.

In TOUGHREACT, the kinetic rate expression for mineral dissolution/precipitation is that of /Lasaga et al. 1994/:

$$r = \pm A\left|1 - \Omega^{\theta}\right|^{\eta} \qquad \text{Equation 4-8}$$

where r is the net precipitation/dissolution rate (moles per unit time), k is the rate constant (mol per unit surface area and unit time), A is the mineral specific surface area per kg of water, Ω^θ is the kinetic mineral saturation ratio, and θ and η are parameters determined from laboratory experiments. Finally, the rate constant is given by the following expression /Xu et al. 2008/:

$$k = k_{25}^{nu}\exp\left[\frac{-E_a^{nu}}{R}\left(\frac{1}{T} - \frac{1}{298.15}\right)\right] + \sum_i k_{25}^{i}\exp\left[\frac{-E_a^{i}}{R}\left(\frac{1}{T} - \frac{1}{298.15}\right)\right]\prod_j a_{ij}^{n_{ij}} \qquad \text{Equation 4-9}$$

where k_{25}^{nu} is the rate constant at 25°C and for the neutral mechanism (mol per unit surface area and unit time), R is the gas constant, T is the absolute temperature in Kelvin, E_a^{nu} is the activation energy for the neutral mechanism, k_{25}^{i} is the rate constant at 25°C for i-th mechanism, E_a^{i} is the activation energy for the i-th mechanism, and a_{ij}^{nij} is the molality of the j-th aqueous species involved in the i-th mechanism.

In the rate constant, besides the so-called neutral mechanism which is solely temperature dependant, several additional mechanisms may be taken into account for the kinetic dissolution/precipitation of a given mineral. pH and dissolved oxygen concentration are some of the most used mechanisms, but the expression for the rate constant in TOUGHREACT accommodates up to five additional mechanisms that can be defined by the user, and each mechanism may involve up to five species /Xu et al. 2008/.

TOUGHREACT does not account for (1) the deformation of the porous skeleton either due to mechanical stress or swelling processes; (2) fluid pressure effects owing to porosity changes; and (3) heat effects from chemical reactions, such as changes in thermo-physical properties of fluids (viscosity, surface tension and density).

4.2 Description of input data

In the LOT A2 test, the bentonite blocks surrounding the copper tube have a radial symmetry. Therefore, a one-dimensional axis-symmetric model was built (Figure 4-1). From the axis of the LOT A2 borehole to the granitic host rock, the heater occupies the first 46 mm, followed by a 4 mm thick copper tube surrounding the heater and, finally, 100 mm of compacted bentonite are placed between the copper tube and the granitic host rock (Figure 4-1). It should be noted that for operational purposes, two small gaps of approximately 0.5 cm were left between the bentonite and the copper tube and between the bentonite and the host rock.

As already mentioned, the LOT A2 test lasted 6 years. During the first year, temperature build up occurred, so that for the subsequent 5 years, the temperature profile in the bentonite blocks was kept stable (Figure 2-2). During the last 5 years of the LOT A2 test, the heater placed inside the copper tube induced a temperature of 130°C at the inner border of the bentonite, and 85°C at the outer border, where the bentonite blocks contact the granitic host rock. In order to simplify the model, this temperature profile has been implemented in our calculations from the beginning.

In addition, at the outer border of the bentonite blocks, a constant water pressure of 1.2 MPa was kept (Figure 4-1). As previously mentioned, the groundwater used to maintain the water pressure stable at the outer border of the bentonite blocks was taken from a borehole drilled in the Äspö HRL /Karnland et al. 2009/.

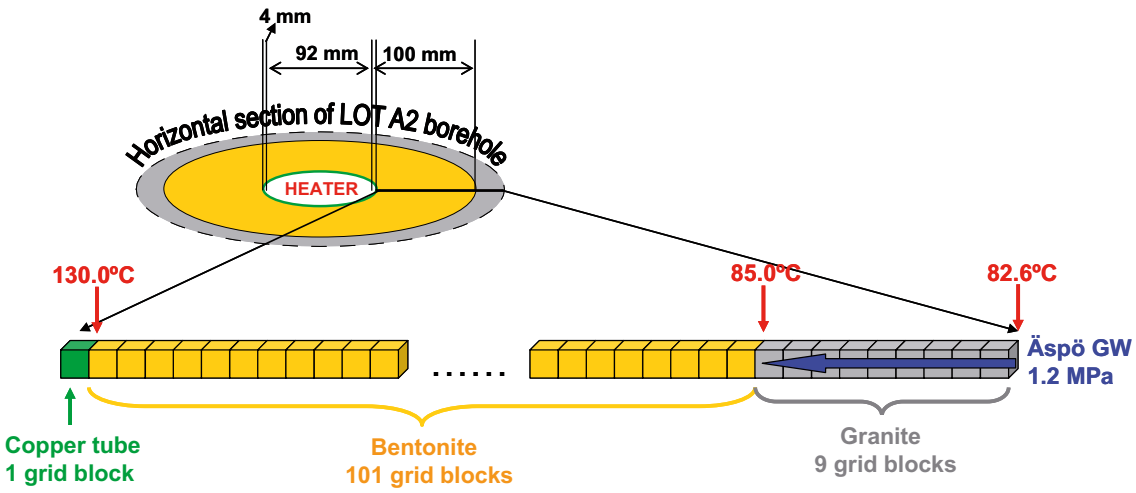

Figure 4-1. *Spatial discretization of the 1D axis-symmetric numerical model and thermo-hydraulic boundary conditions of the LOT A2 borehole, located at the depth of the heater.*

4.2.1 Space and time discretization

The numerical mesh representing the space discretization of the modelled domain is a one-dimensional axis-symmetric finite volume mesh (Figure 4-1), and has been built using the meshmaker option of the TOUGH2 program /Pruess et al. 1999/. The system has been divided in 111 grid blocks of 1 mm each and started at a radial distance of 5 cm (accounting for the heater radius). The following distribution of the grid blocks has been considered, one grid block representing the copper tube, 101 grid blocks representing the compacted bentonite, and the last 9 grid blocks have been assigned to the granite host rock (Figure 4-1).

Calculations reproduce the hydrogeochemical evolution of a system (1) under transient state and, (2) from well-known initial conditions, induced by the imposed environmental boundary conditions. The corresponding hydraulic, thermal and geochemical properties of each grid block have been set according to the three materials considered: copper tube, compacted bentonite, and granite.

A simulation time of 5 years has been implemented, with an initial time step of $1.0 \cdot 10^{3}$ seconds, increasing it automatically until a maximum time step of $1.0 \cdot 10^{7}$ seconds. The convergence criteria imposed in our calculations are in accordance with the suggestions of the code authors /Pruess et al. 1999/:

- 25 as the maximum number of sequential iterations between transport and chemistry,
- 50 as the maximum number of iterations allowed for solving whole geochemical system,
- $1.0 \cdot 10^{-4}$ as the relative tolerance of aqueous concentration for sequential transport/chemistry convergence, and
- $1.0 \cdot 10^{-5}$ as the relative tolerance of aqueous concentration for whole chemical system.

4.2.2 Initial and boundary conditions for the thermo-hydraulic system

As previously mentioned, the numerical model reproduces the hydrochemical evolution of the bentonite blocks of the LOT A2 test during 5 years, considering a constant thermal profile. Initially (and according to the chloride mass balance previously calculated in Section 2.1.4), the initial water saturation of the bentonite blocks has been set to 0.4837. In addition, the whole modelled domain has been considered to be at a total pressure of 0.07 MPa (adopted by model calibration). Exception is made for the grid block located at the right border of the modelled domain (with granite properties), to which a constant water pressure of 1.2 MPa has been assigned. This boundary condition has been set according to the water pressure applied at the outer border of the LOT A2 borehole during the last five years of the experiment /Karnland et al. 2009/.

In order to establish the thermal gradient according to measured data, a temperature of 82.6°C has been imposed to the granite block at the right border of the modelled domain (Figure 4-1), to which a constant pressure of 1.2 MPa has been prescribed. In addition, a constant temperature of 130°C has been assigned to the left border of the modelled domain, representing the copper canister. Under these boundary conditions, the thermal gradient reported for the last 5 years of the LOT A2 test (see Figure 2-2B) is maintained throughout the simulated period.

A second case has been analyzed considering a constant thermal regime at a fixed temperature of 25°C. This model has been performed in order to represent the bentonite evolution in an unheated part of the parcel (block A233BWb; see Section 5.3).

4.2.3 Thermo-hydraulic properties of the modelled domain

In the numerical model of the LOT A2 test, the thermo-hydraulic properties assigned to the compacted bentonite have been set according to data reported in Table 2-5 /Karnland et al. 2009/. In addition, in order to simulate the variably saturated flow in TOUGH2, the values of the parameters that describe (1) the relative permeability function, (2) the capillary pressure function, and (3) the Klinkenberg effect of the compacted bentonite are needed. These parameters have been set according to the calibration procedure explained below.

Since there is no available data for the temporal evolution of the moisture content in the blocks A209BSb and A211BWb, and due to the similarities between the FEBEX experiment and the LOT A2 test, functions for the relative permeability and capillary pressure implemented in the numerical

model of the LOT A2 test are those previously implemented in the numerical model of the FEBEX experiment (Section 3.3): (1) both phases (liquid and gas) are perfectly mobile, and (2) the function of the Leverett's capillary pressure, respectively.

Leverett's function relates the capillary pressure to the water saturation by using a term that is dependant on the temperature /Pruess et al. 1999/:

$$P_{cap} = -P_0 \, \sigma(T) \, f(S_l)$$ Equation 4-10

where:

$$f(S_l) = 1.417\left(1 - S^*\right) - 2.120\left(1 - S^*\right)^2 + 1.263\left(1 - S^*\right)^3$$ Equation 4-11

$$S^* = \frac{S_l - S_{lr}}{1 - S_{lr}}$$ Equation 4-12

and P_{cap} is the capillary pressure, P_0 is the characteristic capillary pressure, $\sigma(T)$ is the surface tension of water (supplied internally in TOUGH2), S_l is the wetting fluid saturation (water in our case) and S_{lr} is the irreducible water content. P_{cap} and S_l are the unknowns that TOUGH2 computes for each time step. The parameters to which we have to assign the characteristic values are P_0 and S_{lr} (0.2 MPa and 0.0, by re-calibration, and assumed from the FEBEX experiment, previously described).

The Klinkenberg effect, for enhancing gas phase permeability, is expressed as follows:

$$k_{gas} = k_{liq}\left(1 + \frac{b}{P}\right)$$ Equation 4-13

where k_{gas} is the absolute permeability for the gas phase, k_{liquid} is the absolute permeability for the liquid phase, b is the Klinkenberg parameter (MPa), and P is the pore pressure (MPa).

The values of the parameters for the relative permeability and capillary pressure functions used in the numerical model of the LOT A2 test have been calibrated by finding the best agreement between measured and simulated data for the content of chloride and sulphate in the blocks A209BSb and A211BWb, at the end of the LOT A2 test. Such calibration has been performed because it is believed that, besides advection, dispersion, and diffusion, the transport of chloride is also influenced by the evaporation/condensation, and suction of the bentonite porewater (as previously shown in the numerical model of the FEBEX experiment; Section 3.3). In addition, the transport of sulphate is also influenced by the dissolution/precipitation of sulphate minerals which, in turn, are influenced by the temperature gradient and the evaporation/condensation cycling for which the parameterization of the relative permeability and capillary pressure functions plays a crucial role.

The calibrated values of the parameters describing the relative permeability function, capillary pressure function and Klinkenberg effect are shown in Table 4-1.

Table 4-1. Values of the thermo-hydraulic parameters assigned to the three grid block materials (copper tube, bentonite, and granite) that constitute the numerical model of the blocks A209BSb and A211BWb (called "Base Case"). (*) The coefficient of molecular diffusion implemented in the isothermal model (block A233BWb, at a constant temperature of 25°C) has been of $1 \cdot 10^{-10}$ $m^2 \cdot s^{-1}$.

Parameter		Copper tube	Bentonite	Granite
Porosity	(–)	$1.0 \cdot 10^{-10}$ [(a)]	0.43 [(b)]	$1.0 \cdot 10^{-3}$ [(c)]
Absolute permeability	(m^2)	$1.0 \cdot 10^{-20}$ [(d)]	$1.0 \cdot 10^{-20}$ [(b)]	$1.0 \cdot 10^{-20}$ [(d)]
*Molecular diffusion coef.	($m^2 \cdot s^{-1}$)	$3.0 \cdot 10^{-8}$ [(d)]	$3.0 \cdot 10^{-8}$ [(e)]	$3.0 \cdot 10^{-8}$ [(d)]
Tortuosity	(–)	1.0 [(d)]	1.0 [(e)]	$1.0 \cdot 10^{-9}$ [(e)]
Thermal conductivity sat.	$W \cdot m^{-1} \cdot °C^{-1}$	388 [(f)]	1.15 [(g)]	1.15 [(d)]
Specific heat capacity	($J \cdot kg^{-1} \cdot °C^{-1}$)	$1.0 \cdot 10^{20}$ [(h)]	964 [(f)]	964 [(d)]
Klinkenberg parameter	MPa	$1.0 \cdot ^{101}$ (d)	$1.0 \cdot 10^{1}$ [(e)]	$1.0 \cdot 10^{1}$ [(d)]

[(a)] Considered very low; [(b)] from /Karnland et al. 2009/; [(c)] same as /Arcos et al. 2003/; [(d)] same as for the bentonite grid blocks; [(e)] model calibration; [(f)] general literature; [(g)] from /Villar et al. 2008b/; [(h)] for prescribing constant temperature boundary condition in the modelled domain.

Since the main objective of the numerical model developed here concerns the geochemical reactions taking place in the bentonite, under the thermo-hydraulic conditions previously described in Section 4.2.2, the parameterization of the relative permeability function, capillary pressure function and the Klinkenberg effect (previously established for the compacted bentonite) has been also attributed to the grid blocks that represent the copper tube and the granite. In addition, the thermal properties attributed to the bentonite grid blocks (Table 2-5) were also attributed to the granite grid blocks.

The thermo-hydraulic parameters assigned to the three materials of the modelled domain are listed in Table 4-1. The specific heat capacity of the grid block representing the copper tube has been set very large ($1.0 \cdot 10^{20}$ J·kg^{-1}·°C^{-1}), in order to ensure a constant temperature boundary condition at this border of the modelled domain. And the fully water saturated thermal conductivity of the copper canister was set to 388 W·m^{-1}·°C^{-1}, according to general literature. In addition, a constant boundary condition for pressure, temperature and water composition has been set to the granite grid block at the right border of the modelled domain. In TOUGHREACT, this type of boundary condition is set by assigning a very large volume to the grid block, where water pressure and composition are intended to be constant over time.

As indicated in Section 3.2.1, the calibrated value of the effective diffusion coefficient implemented in the numerical model of the blocks A209BSb and A211BWb ($3 \cdot 10^{-8}$ m^2·s^{-1}) is higher than the maximum value reported for laboratory conditions (between 10^{-9} and 10^{-10} m^2·s^{-1}, /Karnland et al. 2009/), due to the high temperatures under which the LOT A2 test has been performed. On the other hand, the estimated value of 10^{-10} m^2·s^{-1} has been implemented in the isothermal model of the block A233BWb, under a constant temperature of 25°C.

As previously explained, TOUGHREACT does not compute the hydrodynamic dispersion as a Fickian diffusion analogue and, therefore, dispersion is not defined as an input data in the numerical model. Instead, it is calculated internally through a spatial resolution on multiple scales. Under this premise, the Peclet number is always fulfilled.

4.2.4 Initial and boundary conditions for the hydrochemical system: initial porewater composition and boundary inflow

The initial porewater for the bentonite materials included in our calculations corresponds to the water composition estimated from the aqueous leachates performed by UniBern /Karnland et al. 2009/, using the methodology described in Section 2.1.2 (Table 4-2). Since the copper tube reactivity has been ignored in the present exercise, the composition of the initial porewater of the grid block representing the copper tube is set equal as in the bentonite grid blocks.

The composition of the Äspö groundwater injected at the right border of the modelled domain is the one measured from samples collected from borehole HG0038B01, drilled in the Äspö tunnel (Table 4-2). The composition of the granite grid block at the right border of the modelled domain is set constant over time, in order to properly simulate the continuous inflow of Äspö groundwater at the periphery of the LOT A2 borehole. The composition of the initial porewater of the grid blocks representing the granite also corresponds to the sampled Äspö groundwater.

Table 4-2. Composition of the Äspö groundwater (Äspö GW, taken from borehole HG0038B01) that supplied the LOT A2 test and the reference porewater, A213 (prior to the heating test; /Karnland et al. 2009/). Water compositions used in the numerical model developed here.

Parameter	Äspö GW (mol·L^{-1})	A213 (mol·L^{-1})
pH	6.9	7.859
Ionic strength	$2.5 \cdot 10^{-1}$	$2.76 \cdot 10^{-1}$
Cl	$1.78 \cdot 10^{-1}$	$4.00 \cdot 10^{-2}$
Na	$9.60 \cdot 10^{-2}$	$2.12 \cdot 10^{-1}$
K	$2.60 \cdot 10^{-4}$	$1.40 \cdot 10^{-3}$
Ca	$5.60 \cdot 10^{-2}$	$1.01 \cdot 10^{-2}$
Mg	$1.60 \cdot 10^{-3}$	$5.81 \cdot 10^{-3}$
SO_4^{2-}	$6.00 \cdot 10^{-3}$	$9.65 \cdot 10^{-2}$
HCO_3^-	$4.40 \cdot 10^{-4}$	$1.05 \cdot 10^{-3}$
Si	$1.60 \cdot 10^{-4}$	$6.25 \cdot 10^{-3}$

4.2.5 Geochemical properties and processes

In the numerical model developed here only bentonite is considered to have reactive minerals (Table 4-2).

As shown in Table 2-3, two sulphur-bearing solid phases are present as primary mineral assemblage of the bentonite blocks: gypsum and pyrite. These imply two oxidation states for sulphur: S(VI) in gypsum and S(-II) in pyrite. Evidences from previous numerical modelling exercises /Arcos et al. 2003, 2008/ and also from the LOT A2 results /Karnland et al. 2009/, show that kinetics of pyrite dissolution during the water saturation stage of the bentonite blocks should be very slow under the pH and redox conditions that prevailed during the LOT A2 test. Therefore, pyrite was not considered in the model. Under this premise, the redox state of the chemical system modelled here can be discarded from the simulations, since the rest of geochemical reactions considered in the LOT A2 model do not involve changes in the redox state of the chemical species.

Opposite to what was stated for pyrite, gypsum is expected to have a very fast reactivity under the thermo-hydraulic and chemical conditions that prevailed during the LOT A2 test. At the temperature range considered in the model representative of the blocks A209BSb and A211BWb (130°C to 85°C), anhydrite is the thermodynamically stable Ca-sulphate phase. Therefore, the pool of gypsum (identified in the bentonite under the laboratory conditions) has been modelled as anhydrite, under local equilibrium. However, at the temperature range representing the thermal behaviour of the block A233BWb (25°C), gypsum is the thermodynamically stable Ca-sulphate phase. Feldspar, mica, and montmorillonite (the other three minerals identified in the bentonite rings; Table 2-3), are expected to have very slow kinetics under the thermo-hydraulic and chemical conditions of the LOT A2 test, and therefore, no reactivity has been attributed to these minerals.

The results of the LOT A2 test show that the structure of montmorillonite was kept relatively unchanged /Karnland et al. 2009/. Therefore, montmorillonite only participates on cation exchange reactions in the numerical model, and the total number of exchange sites is kept constant throughout the simulation. The model for cation exchange is that of /Bradbury and Baeyens 2003/. The selectivity coefficients of the exchangeable cations are listed in Table 4-4.

The precipitation of secondary minerals, such as calcium sulphates, carbonates and silica, is most likely triggered under the high temperatures that prevailed during the experiment, as previously argued in Section 3.2.2. In this context, if oversaturation is reached, calcite, anhydrite and silica are allowed to precipitate under local equilibrium (Table 4-2).

Table 4-3. Summary of the reactive mineral reactions considered in the numerical simulations in the bentonite.

Mineral	Initial concentration (wt%)	Reaction type	Species involved in: – Cation exchange
Anhydrite	0.283	Diss./prec. under local equilibrium	
Montmorillonite	0.75 eq·kg^{-1} of bulk bentonite	Cation exchange under local equilibrium	Na^+, K^+, Mg^{2+}, Ca^{2+}
SiO_2(am)	5.0	Diss./prec. under local equilibrium	
Calcite	–	Diss./prec. under local equilibrium	

Table 4-4. Cation exchange reactions implemented in the numerical model, according to the cation exchange model proposed by /Bradbury and Baeyens 2003/.

Reaction	Log K
$X^- + Na^+ = NaX$	0.00
$X^- + K^+ = KX$	0.60
$2X^- + Ca^{2+} = CaX_2$	0.41
$2X^- + Mg^{2+} = MgX_2$	0.34

5 Numerical results

Since the objective of the present work is to assess the influence that the thermo-hydraulic processes exert on the geochemical behaviour of the bentonite, the thermal scenario considered as the "Base Case" is focused on the standard bentonite blocks located at 3 m depth (A209BSb and A211BWb), where the highest thermal gradient was registered (Figure 2-1). The thermal scenario and the parameters defining this case are described in Section 4.2 (Table 4-1 and Table 4-2). In addition to the Base Case, a sensitivity analysis has been performed in order to assess the influence of the variability of some "key" parameters on the numerical results. These key parameters are:

- the initial water saturation;
- the initial amount of gypsum (as a primary mineral phase in bentonite);
- the water pressure applied on the granite boundary; and,
- the diffusion coefficient implemented in the whole domain.

Finally, the results obtained in the Base Case have been compared with those obtained in a section at a constant temperature of 25°C (block A233BWb).

5.1 Base Case

5.1.1 Water saturation and temperature of the bentonite blocks

The numerical results indicate that the bentonite was practically water saturated within the first year (Figure 5-1). These calculations are in agreement with the observations made during the LOT A2 test.

The saturation process depends on (1) the thermo-hydraulic properties assigned to the three grid block materials of the modelled domain, which were described in Section 4.2.3 (Table 4-1 and Table 4-2), and on (2) the thermo-hydraulic initial and boundary conditions, which were described in Section 4.2.2. In this way, the final time of the fully water saturation is very sensitive with respect to slight variations of the external pressure. This is a remarkable aspect calibrating the numerical model.

As a consequence of the water evaporation in the vicinity of the copper tube, the water saturation of the bentonite drops to close to 0.0 during the first 10 days (Figure 5-1). The evaporation front advances during the first half-year, reaching a distance of 2 cm from de copper tube. Thereafter, the pressure supplied at the right border of the modelled domain (granite) exceeds the vapour pressure at the vicinity of the copper tube, leading to the gradual saturation of the bentonite. Associated to the evaporation front, an increase of the initial water content has been calculated as a consequence of the condensation of the water vapour (Figure 5-1). This condensation effect evolves in parallel to the evaporation during the first half-year and, thereafter, it is minimized by the effect of the external water injection.

After 0.6 years, the saturation front draws a vertical sharp that divides the portion of bentonite which is fully saturated and the fully dry portion. Finally, bentonite is practically fully saturated after 1 year.

The thermal gradient computed for the modelled domain (Figure 5-1) is in agreement with reported observations, when the analytical profile of temperature was kept stable (Figure 2-2B).

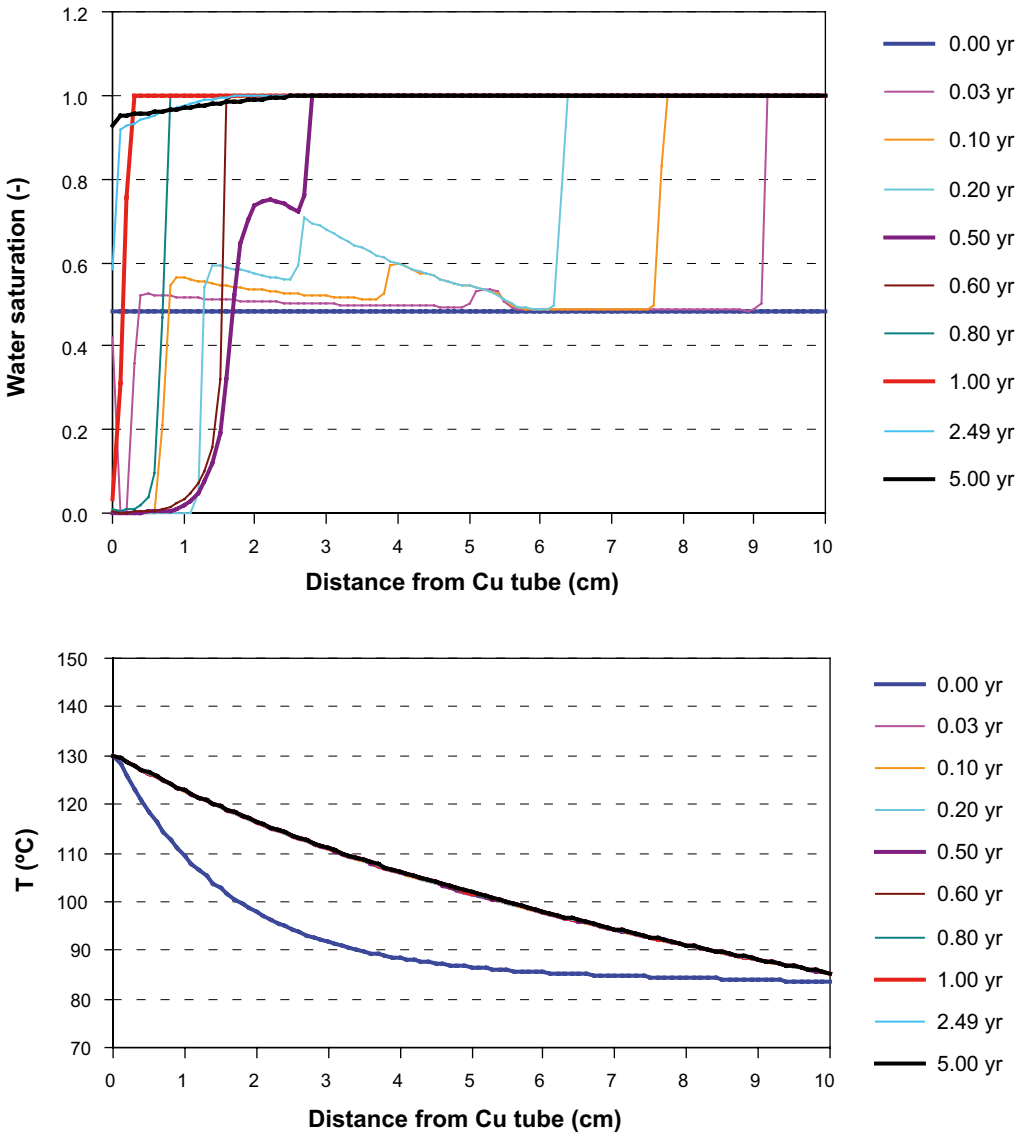

Figure 5-1. *Computed evolution of water saturation and temperature of the bentonite blocks, located at the depth of the heater of the LOT A2 test.*

5.1.2 Transport of chloride

Under the geochemical and thermo-hydraulic conditions that prevailed during the LOT A2 test, and despite the fact that the bentonite porewater evaporates at the vicinity of the copper tube during the first year, numerical results indicate that no chloride salts precipitate and, therefore, chloride behaves conservatively. Under this premise, chloride mobility in the bentonite blocks depends solely on (1) mixing between the two waters involved in the LOT A2 test, and on (2) the flow of water during the saturation period of the bentonite blocks. In this way, the flow of water in the bentonite blocks is influenced by the water pressure applied at the periphery of the borehole, and by the evaporation/condensation cycles that occurred during the early stages of the experiment. Therefore, the hydraulic parameters and the effective diffusion coefficient assigned to the grid blocks representing the bentonite and granite exert a great influence on the simulated evolution of chloride concentration.

Numerical results agree well with data on chloride concentration measured in the aqueous leachates extracted from blocks A209BSb and A211BWb, at the end of the LOT A2 test (Figure 5-2).

Calibration of the effective diffusion coefficient was performed by searching for the best agreement between simulated and measured chloride concentrations at the end of the experiment (Figure 5-2). The corresponding molecular diffusion coefficient is $3 \cdot 10^{-8}$ $m^2 \cdot s^{-1}$, and the tortuosity attributed to the bentonite grid blocks is 1.0. In order to properly simulate the transition between the chloride

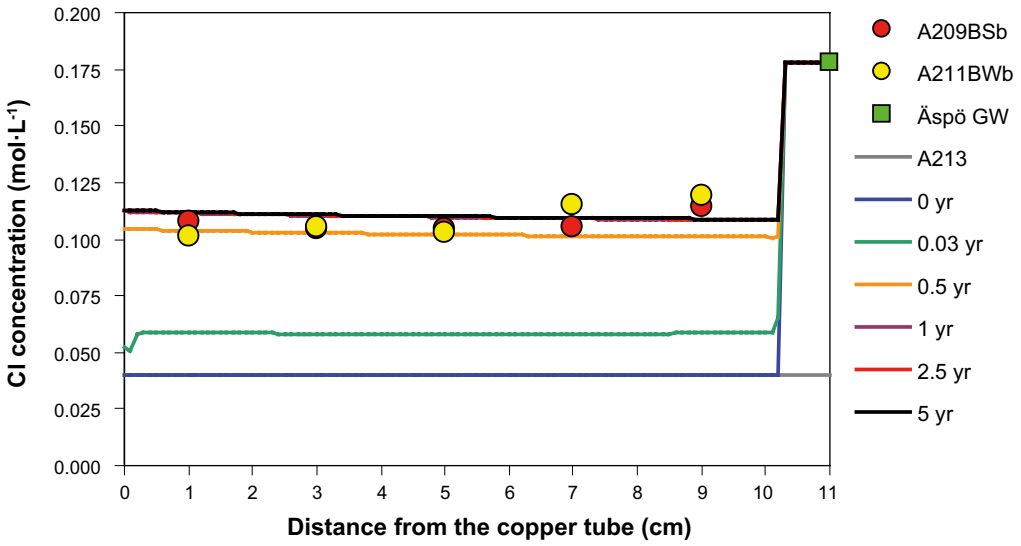

Figure 5–2. *Computed evolution of chloride concentration in the modelled domain, and analytical data from A209BSb and A211BWb samples.*

concentration measured in blocks A209BSb and A211BWb, and the concentration of chloride in the Äspö groundwater, which was fixed 1 cm away from the contact with the bentonite, a tortuosity of $1.0 \cdot 10^{-9}$ was assigned to the granite. Therefore, using this very low tortuosity in the granite material, we can achieve that the Cl diffusion was only effective within of the bentonite porosity.

5.1.3 Transport of reactive solutes and geochemical reactions

Numerical results for the aqueous concentration of cations, such as Na^+ and Ca^{2+}, do not agree with data from the aqueous leachates performed for the bentonite blocks A209BSb and A211BWb at the end of the LOT A2 experiment. The reason for this disagreement is related to the changes induced in the exchanger during the leachate test, as explained previously (Section 2.1.2). Therefore, the comparison between numerical results for the aqueous cations and the experimental results of the aqueous leachates has inevitably a high degree of uncertainty. Nevertheless, computed results for the composition of the cation exchanger agree with the experimental results at the end of the LOT A2 test. According to /Karnland et al. 2009/, in the hot blocks:

- exchangeable Na^+ has been replaced by Ca^{2+}, in the area close to the copper tube and,
- exchangeable Mg^{2+} increases with increasing temperature.

On the contrary, sulphate is the reactive component that can be better used to evaluate our conceptual model, as it is involved in the same transport processes as chloride and, additionally, in the dissolution-precipitation of anhydrite. Moreover, during the leachate tests, anhydrite is assumed to be fully dissolved and, therefore, the leachate data will represent the sum of both aqueous sulphate from porewater and dissolved calcium sulphate.

Anhydrite equilibrium, within the whole range of temperatures, is the process controlling the distribution of S(VI) aqueous species and the total sulphate content of the samples (Figure 5-3). The initial aqueous sulphate in porewater is affected by:

1. an increase of concentrations in the vicinity of the copper tube, as a consequence of evaporation, and a relative dilution behind the evaporation front, due to the condensation of water vapour,
2. dilution as a result of the injection of the less concentrated Äspö groundwater (undersaturated with respect to anhydrite),
3. an increase of the sulphate aqueous concentration due to anhydrite dissolution in parallel to bentonite hydration (Figure 5-3), and
4. an increase of the sulphate aqueous concentration in the warmer part of the bentonite due to decrease of the anhydrite solubility.

This sequence of events is relative. In spite of these processes, the aqueous sulphate concentration remains relatively stable, as a consequence of the non-isothermal equilibrium with respect to anhydrite. On the othe hand, the plot of the amount of anhydrite volume (Figure 5-3) shows as anhydrite precipitation mainly occurs when the saturation and the evaporation fronts interact (from 0.5 years). Really, S(VI) concentration is controlled by anhydrite equilibrium, whereas anhydrite had not been depleted.

The trend of the analytical data for the sulphate concentration of the aqueous leachates is well reproduced when the model computes the exhaustion of the primary anhydrite in bentonite between 4.5 and 10 cm from the copper tube (Figure 5-4). Nevertheless, for such a good agreement between measured sulphate in aqueous leachates and computed anhydrite content, the initial amount of sulphate mineral had to be recalculated in the model on a mass balance basis. This calculation has been performed using leachate data and assuming that total sulphate is the sum of aqueous sulphate in porewater and sulphate from anhydrite, and that this mineral was initially homogeneously distributed in the bentonite. The sensitivity of the results with respect to the initial amount of anhydrite will be discussed in Section 5.2.2.

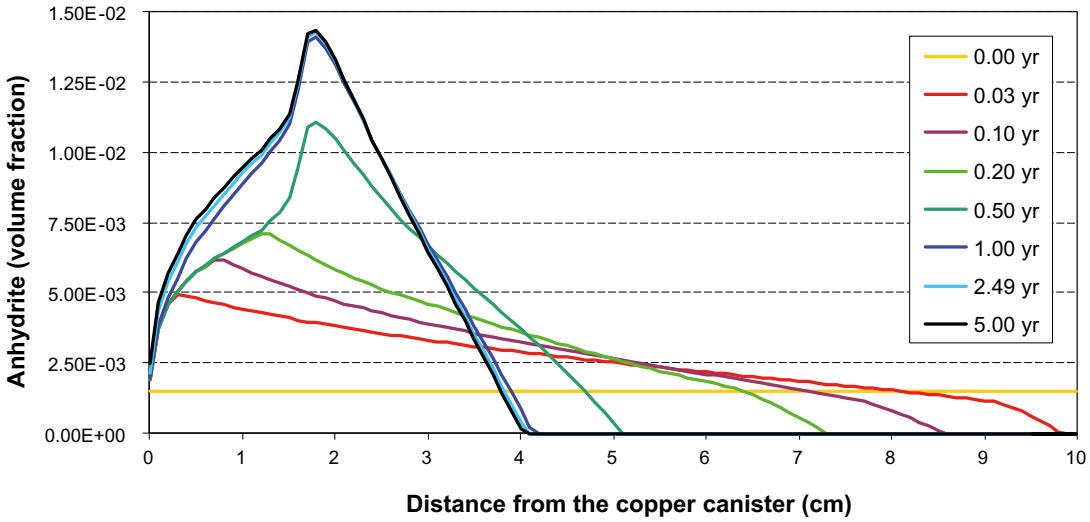

Figure 5-3. *Computed evolution of the volumes of dissolved or precipitated anhydrite, for the Base Case described in Section 5.1.*

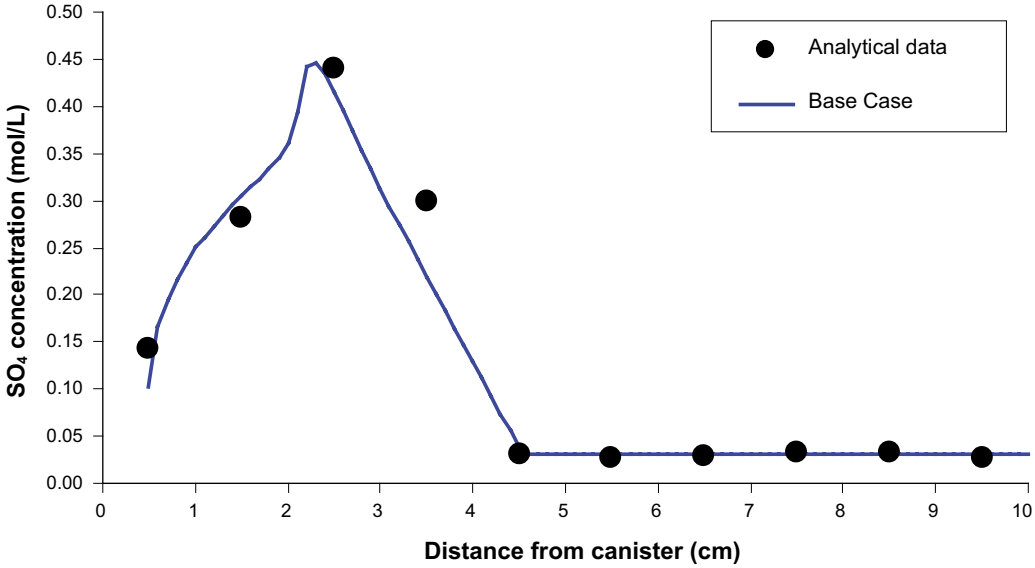

Figure 5-4. *Computed evolution of sulphate content in the modelled domain, and analytical data from A218BSE, analyzed by VTT /Karnland et al. 2009/. As it has been commented previously (Section 3.2), the coordinates of the numerical results have had to be displaced 0.5 cm to be able to compare with the analytical data (as a consequence of the existence of a gap between the copper tube and the bentonite blocks).*

The content of the sulphate measured in the A211BWb block after the test (Figure 5-4) shows that anhydrite precipitation prevails between 0.0 and 4.5 cm of the model (measured from the gap between the copper tube and the bentonite), with a maximum value around 3 cm, that reflects the maximum advance of the evaporation front (Figure 5-1). This trend is a result of the redistribution of anhydrite in the bentonite as a consequence of (1) a decrease of anhydrite solubility as temperature increases, and (2) the transport of sulphate from dissolved anhydrite in the hydrated bentonite further to the warmer part of the system.

The evolution of the amount of silica and calcite precipitated and/or dissolved is shown in Figure 5-5. As it was expected, silica dissolves in the warmer part of the system (especially in the evaporation front) and precipitates in the colder part of the system. On the other hand, the amount of calcite dissolved or precipitated is clearly negligible. It precipitates during the first stages of the calculations due to the increase of temperature. Subsequently, this secondary calcite is re-dissolved by the granite groundwater injected from the external boundary of the bentonite and, also, as a consequence of anhydrite precipitation (in competition for calcium).

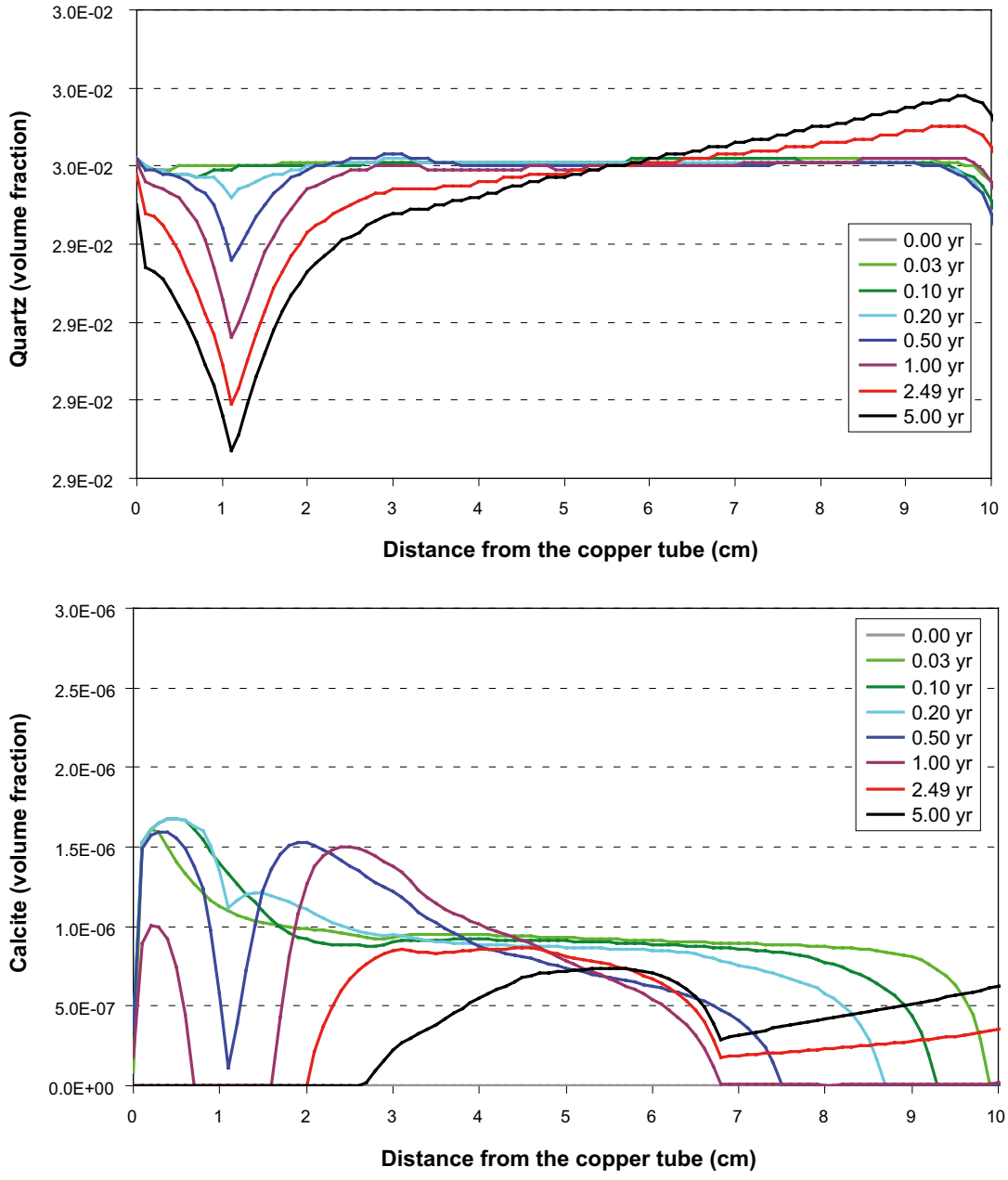

Figure 5-5. *Computed evolution of the volumes of mineral dissolution or precipitation for the Base Case described in the Section 5.1.*

5.2 Sensitivity cases

As indicated previously, a series of sensitivity cases has been performed in order to evaluate the influence on the results of the uncertainty of some parameters: the initial porewater saturation, the amount of primary calcium sulphate in bentonite, the water pressure applied in the bentonite-granite boundary, and the effective values for the molecular diffusion coefficient. In Table 5-1 a summary of the parameters analysed in the sensitivity cases developed for the numerical simulations of the LOT A2 test is presented.

5.2.1 Initial water saturation

The initial water saturation of the bentonite blocks is a parameter which has been evaluated by different methodologies: (1) using the data on the initial water content in the bentonite blocks, and (2) by a mass balance of Cl in the samples analyzed after 5 years of the beginning of the test (when the bentonite is completely water saturated). Both methodologies lead to similar results for the initial water saturation of the bentonite. However, a sensitivity analysis of the results with respect to the variability of this parameter has been performed in order to assess the impact of this uncertainty on numerical results (Figure 5-6).

Table 5-1. Summary of the parameters analysed in the sensitivity analysis of the numerical simulations developed for the heated bentonite.

		Initial water saturation (unitless)	Initial amount of Ca-sulphate (wt%)	Inflow pressure (MPa)	Molecular diffusion coefficient ($m^2 \cdot s^{-1}$)
Base Case (BC)		0.4837	0.283 (anhydrite)	1.2	$3 \cdot 10^{-8}$
Sensitivity cases	**Initial water saturation**	0.4000 0.5500	same as BC	same as BC	same as BC
	Initial amount of Ca-sulphate	same as BC	no Ca-sulphate 0.094 (anhydrite) 0.471 (anhydrite)	same as BC	same as BC
	Inflow pressure	same as BC	same as BC	1.0 1.4	same as BC
	Molecular diffusion coefficient	same as BC	same as BC	same as BC	$8 \cdot 10^{-8}$ $8 \cdot 10^{-9}$

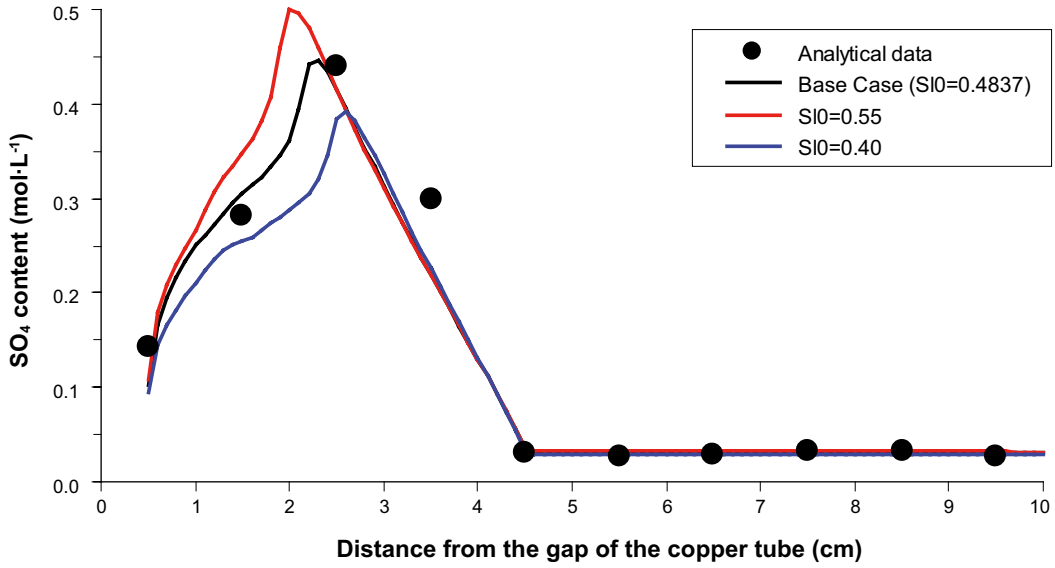

Figure 5-6. *Trend of the sulphate content, calculated for three different initial porewater saturations. The numerical results has been compared with the analytical data from A218BSE, analyzed by VTT /Karnland et al. 2009/.*

In spite the fact that the final content of Cl analyzed does not allow a wide range of variability in the initial water saturation of the bentonite blocks, computed results for an initial water saturation between 0.40 and 0.55 could adjust relatively well to the analytical sulphate content (Figure 5-6). However, as it has been explained previously, the value that better adjusts with the concentrations of Cl measured at the end of the LOT A2 test (S_r = 48.37%) has been selected for the Base Case.

The numerical results show that if the initial water saturation is lower than that considered in the Base Case, a decrease of the amount of sulphate in the warmer part of the domain occurs (Figure 5-6). This is because more anhydrite is needed to dissolve into porewater to reach equilibrium (the Äspö groundwater entering into the system is more diluted than the initial bentonite porewater). On the contrary, if a higher initial saturation degree is considered, less anhydrite is needed to dissolve to reach equilibrium.

On the other hand, the location of the peak of sulphate is controlled by the relative advance of the evaporation and the saturation fronts and they depend on the initial water saturation.

5.2.2 Initial amount of Ca-sulphate

The amount of the Ca-sulphate as a primary component of the bentonite blocks is a "key" parameter when adjusting computed results to the analytical data. In general, the results show a specific sensitivity with respect to the variability of this parameter.

Since it will be commented in Section 5.3, two different average compositions have been adjusted for two different sections (blocks A209BSb-A211BWb and A233BWb). In this context, a sensitivity analysis has been performed, modifying slightly the content initially considered for the Base Case, up to considering a block of bentonite without Ca-sulphate as a primary mineral (Figure 5-7).

As it is predictable, as lower is the amount of anhydrite in the bentonite, more rapidly it will be exhausted in the hydrated part of the bentonite. Consequently, the amount of the aqueous sulphate transported towards the front of evaporation (and the amount of anhydrite able to precipitated here) decrease (Figure 5-7).

It is necessary to emphasize that the approximation that better adjusts to the analytical results is that considered as the Base Case (0.283 wt% anhydrite, for the A211BWb block, and 0.515% wt. gypsum, for the A233BWb block). These values are lower than those estimated by /SKB 2004/ (Table 2-3) and similar to those reported by /Arcos et al. 2003/.

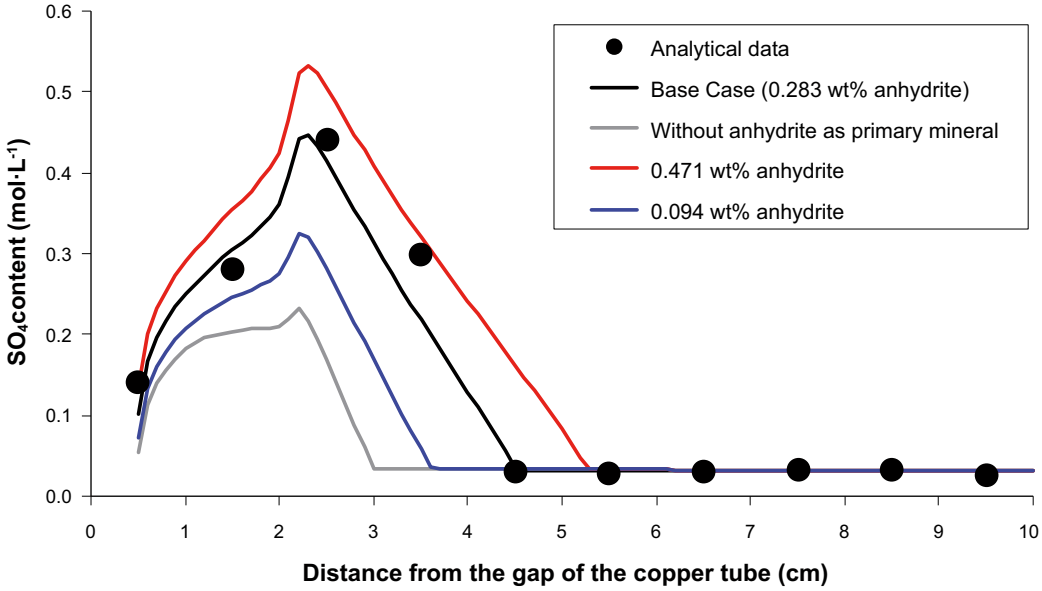

Figure 5-7. *Trend of the sulphate content calculated in four mineralogical scenarios (with respect to the initial amount of Ca-sulphate in the bentonite). The numerical results have been compared with the analytical data from A218BSE, analyzed by VTT /Karnland et al. 2009/.*

The results indicate that the evolution of the total sulphate in the system behaves very similarly in all cases, the main difference is related to the amount of anhydrite precipitated in the warmer part of the bentonite block. In the case when Ca-sulphate does not exist initially as a reactive mineral in the bentonite, the amount of anhydrite precipitated in the warmer part will be half of that calculated for the Base Case.

5.2.3 Water pressure applied at the granite boundary

The pressure supplying aqueous solution through the external boundary of the bentonite is a well-known value (1.2 MPa; /Karnland et al. 2009/). However, due to some incidences that can occur during the test, a sensitivity analysis of the results with respect to the variability of this parameter has been performed.

In general, slight variations of the reference value or increasing pressure do not produce significant differences in the calculated sulphate evolution. However, if the induced pressure is not sufficient to reach water saturation during the modelled time (e.g. a pressure of 1.0 MPa), the amount of anhydrite precipitated drastically changes (Figure 5-8). In this case, the amount of mineral accumulated in the evaporation front increases, induced by a continuous process of water evaporation-mineral precipitation.

5.2.4 Molecular diffusion coefficient

As previously mentioned (in Section 4.1), the effective diffusion coefficient in TOUGHREACT is obtained by multiplying the molecular diffusion coefficient by the tortuosity and porosity, which are explicitly introduced in the input files. In TOUGHREACT, a single value of molecular diffusion is assigned to the whole modelled domain, but the tortuosity and porosity values can be assigned to each of the geologic materials that are present in the modelled domain. Therefore, each material can have a different effective diffusion coefficient. Knowing that the effective diffusion coefficient for chloride and sodium of the compacted bentonite varies between $5 \cdot 10^{-14}$ and $1 \cdot 10^{-9}$ $m^2 \cdot s^{-1}$ at 25°C /Ochs et al. 2006, Bourg et al. 2008, González Sánchez et al. 2008, Kozaki et al. 2008/, the calibrated coefficient obtained in the numerical model ($3.0 \cdot 10^{-8}$ $m^2 \cdot s^{-1}$) is within the range expected considering the thermal field implemented in the Base Case, 130–85°C (see Section 3.2.1). Due to the uncertainty associated to the estimation of this parameter (it has been used as a calibration parameter of the model), an analysis has been performed in order to check the sensitivity of the results with regard to its variability (Figure 5-9).

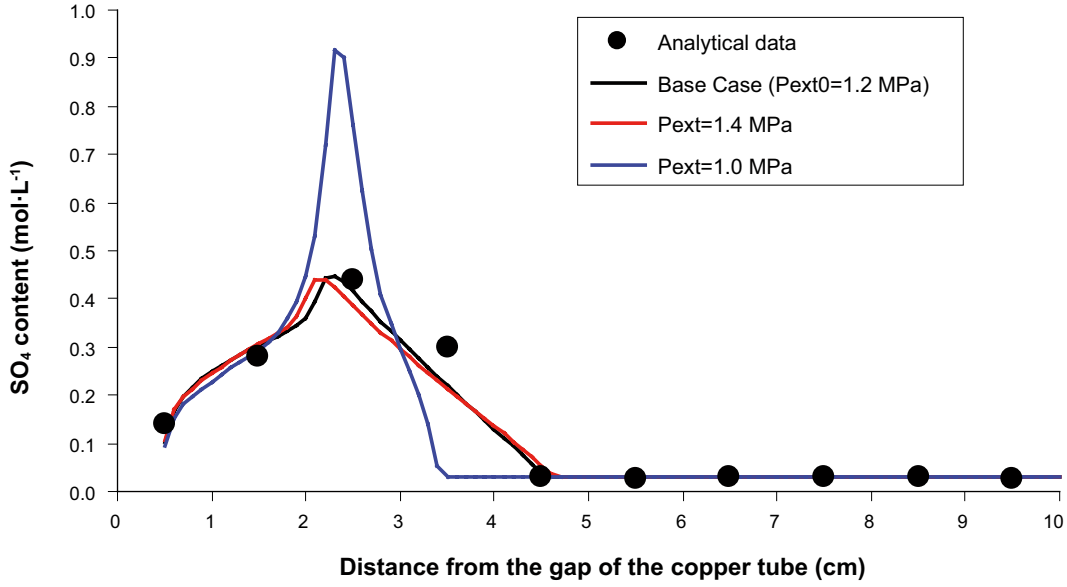

Figure 5-8. *Final total sulphate content, calculated in three water pressure scenarios. The numerical results has been compared with the analytical data from A218BSE, analyzed by VTT /Karnland et al. 2009/.*

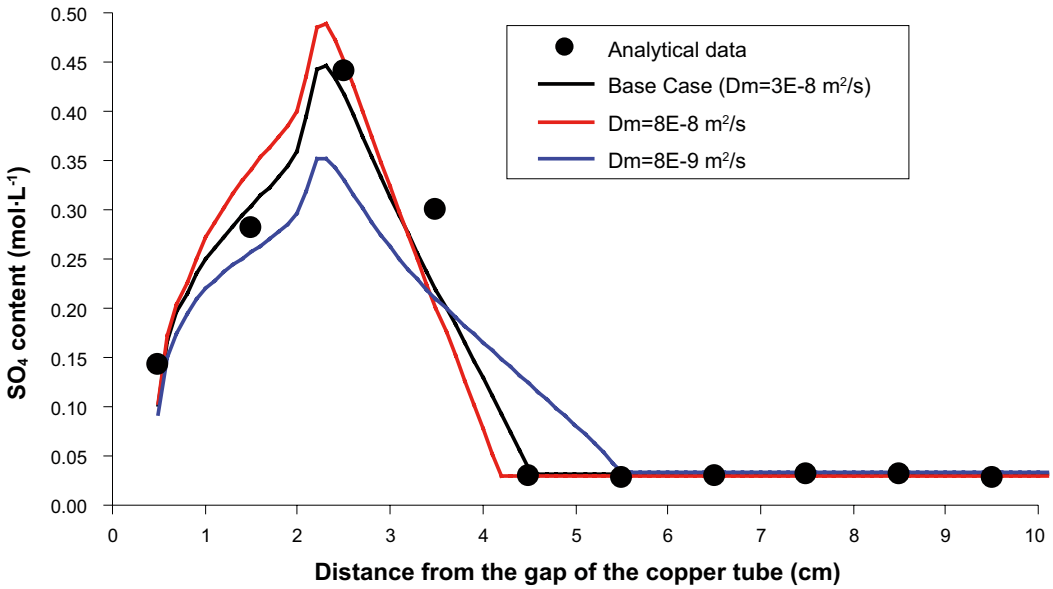

Figure 5-9. *Trend of the SO_4 content calculated for three molecular diffusion coefficients. The numerical results has been compared with the analytical data from A218BSE, analyzed by VTT /Karnland et al. 2009/.*

Decreasing the diffusion coefficient leads to the decrease of the anhydrite dissolved in the "cold" domain of the model. This produces a decrease of the aqueous sulphate species, and its subsequent transport to the warm part of the domain is delayed. Therefore, the amount of anhydrite precipitated decreases and is distributed through a wider zone (Figure 5-9). On the contrary, higher values for the diffusion coefficient lead to the increase of the dissolution of the primary Ca-sulphate in the bentonite materials. Therefore, higher amounts of aqueous sulphate species are transported towards the evaporation front, where higher amounts of anhydrite precipitate (Figure 5-9).

5.3 Block A233BWb – an isothermal section with a constant temperature of 25°C

A numerical model reproducing a block of bentonite at a constant temperature of 25°C has been performed in order to describe the geochemical evolution of a section of bentonite under non-heated conditions (block A233BWb, i.e.; Figure 2-1, Figure 2-2b), and to allow the comparison with the high temperature model.

The main conceptual differences with respect to the Base Case described in the previous section are (Table 5-2):

- the Ca-sulphate in equilibrium with the new thermal scenario is gypsum, instead of anhydrite,
- new thermal boundary conditions have been implemented in order to ensure a constant temperature of 25°C in grid blocks,
- a molecular diffusion coefficient of 10^{-10} $m^2 \cdot s^{-1}$ has been implemented, in accordance with the values discussed above.

Table 5-2. Summary of the parameters that have been used to calibrate the numerical results in the Base Case and in the Isothermal Case.

	Temperature range (°C)	Initial amount of Ca-sulphate (wt%)	Molecular diffusion coefficient ($m^2 \cdot s^{-1}$)
Base Case	85 to 130	0.283 (anhydrite)	$3 \cdot 10^{-8}$
Isothermal Case	25	0.515 (gypsum)	$1 \cdot 10^{-10}$

In this case (as it occurred in the previous case), the initial amount of gypsum has been also recalculated on a mass balance basis using data from leachate tests for block A233BWb, resulting in an initial amount of gypsum of 0.515 wt%. Using this initial amount of gypsum, the calculated evolution of the total sulphate is in agreement with the analytical data (Figure 5-10).

At 25°C, the saturation process of the bentonite blocks is substantially slower than the Base Case (Figure 5-10, Figure 5-1). In the vicinity of the copper tube, water saturation remains practically constant because there is no evaporation. Under these conditions, suction is less pronounced than in the high temperature (and non-isothermal) Base Case. The capillary pressure is a function of the surface tension of water (which is also a function of temperature) and of the water saturation of the sample /Leverett 1941, Udell and Fitch 1985/. In this context, and under the same conditions of external pressure, the heated bentonite block will become saturated faster than the unheated bentonite block (Figure 5-1, Figure 5-11).

Figure 5-11 also illustrates the evolution of the content of the conservative Cl, with a significant delay with respect to that described for the non-isothermal Base Case (Figure 5-1). This is a consequence of the previously mentioned lower efficiency of the saturation process at low temperatures. On the other hand, as a result of the low molecular diffusion coefficient implemented, the Cl content within the bentonite shows the existence of intermediate gradients of concentrations.

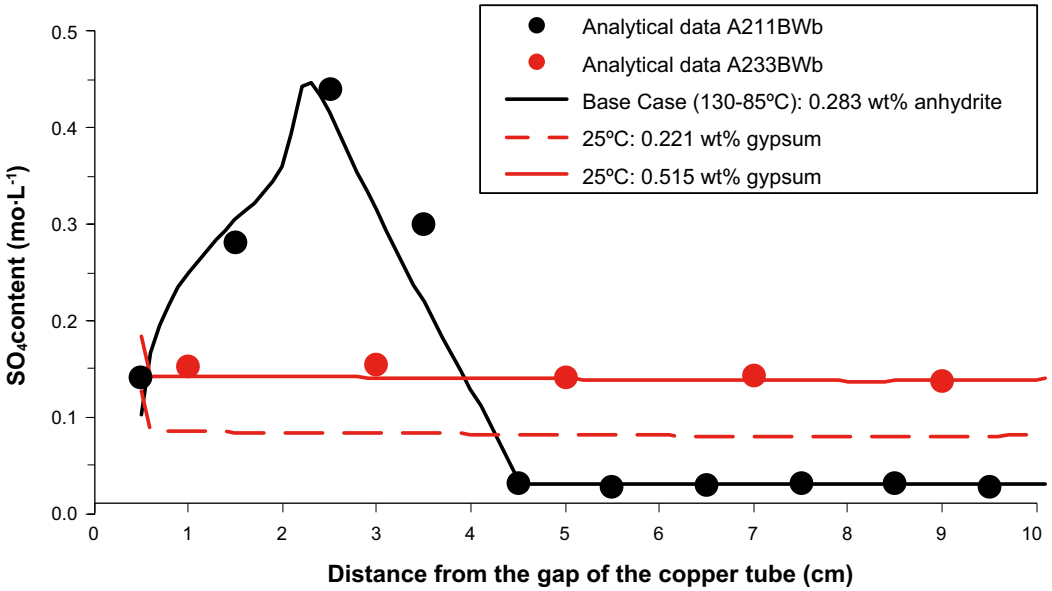

Figure 5-10. *Computed content of sulphate in the heated (A211BWb, in black) and non-heated (A233BWb, in red) bentonite blocks.*

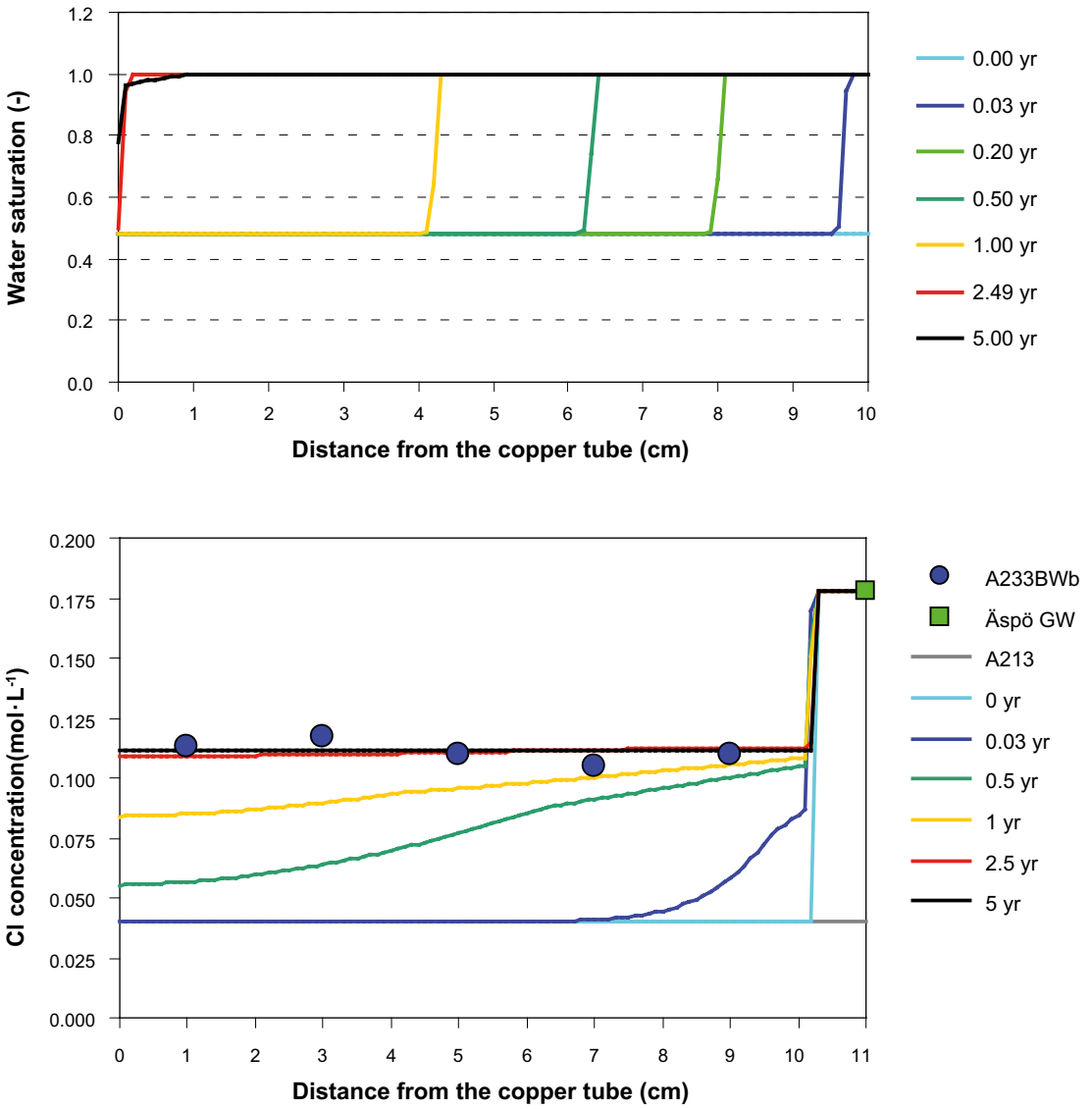

Figure 5-11. *Distribution of water saturation and Cl content calculated for the isothermal model representative of the block A233BWb.*

6 Conclusions

The results of the numerical simulations developed here have led to an overall good agreement with data measured in the LOT A2 test. This agreement proves the validity of the conceptual model defined for this experiment, and also helps us to identify those parameters for which higher degrees of uncertainty prevail.

The parameters that influence the evolution of water saturation of compacted bentonite under a high thermal gradient have been thoroughly discussed and tested in the numerical simulations. The functions and corresponding parameters for the relative permeability and capillary pressure, together with the Klinkenberg parameter, of the compacted bentonite play a crucial role in the computed evolution of water saturation. When modelling the thermo-hydraulic behaviour of the compacted bentonite, it has been concluded that the movement of the gas and liquid phases is better modelled when these are assumed perfectly mobile. In addition, although different functions have been applied in the numerical model of the column experiment conducted by Ciemat with FEBEX bentonite /Villar et al. 2008b/, we have attained better results when applying the Leverett's capillary function in TOUGHREACT.

Both experimental and numerical results have proven that the transport of chloride in the compacted bentonite is mainly influenced by the (1) advective flow of the water injected in the bentonite which reflects a piston like flow; (2) the cyclic evaporation/condensation process that occurs in the moving wetting front; and (3) water suction close to the heater. Although Donnan equilibrium and anion exclusion processes are known to influence the transport of chloride in compacted bentonite /Birgersson and Karnland 2009, Muurinen et al. 2004/, the numerical simulations performed have proven that, under the thermo-hydraulic conditions of the LOT A2 test, these processes can be considered of low importance. Little differences in the estimations of some parameters, such as the initial water saturation, could indicate that Donnan equilibrium effects could be at play /Birgersson and Karnland 2009/. In spite of this, for initial water saturation ranged between 0.40 and 0.55 (Figure 5-6), these processes seem to have a negligible influence on the solute distributions.

Besides being influenced by the same processes as chloride, sulphate is also influenced by the precipitation and dissolution of soluble calcium-sulphates which, in turn, are influenced by cation exchange in the montmorillonite interlayer and the evaporation and condensation of porewater. Numerical results for the redistribution of sulphate minerals agree very well with data measured at the end of the LOT A2 test.

When developing the numerical simulations, chemical data from the aqueous leachates performed prior and at the end of the LOT A2 test /Karnland et al. 2009/ have been used to define the initial composition of the bentonite porewater and also to compare with the computed results at the end of the LOT A2 test. The attained results indicate that data from aqueous leachates are the sum of aqueous species and species from the solid phase of the bentonite (both in the exchanger and in accessory minerals) which have been transferred into the aqueous phase during the process of acquisition of the aqueous leachates. These results reflect the need for the development of improved methodologies for assessing the chemical composition of the porewater of a compacted bentonite.

The Base Case developed here corresponds to the numerical simulation that best fits data measured for water saturation, and concentration of chloride and sulphate. Whenever available, thermo-hydraulic and hydrochemical data from /Karnland et al. 2009/ have been used to develop this numerical simulation. The initial mineralogy of the bentonite is taken from /SKB 2004/. Exception is made for the initial amount of Ca-sulphate in the bentonite which had to be set to a lower value than reported based on mass balance calculations using analytical data of the LOT A2 test. This process reflects the fact that, quantification based on X-Ray Diffraction data is semi-quantitative and transformation of gypsum into anhydrite during the thermal test, can result in lower dissolution of this mineral during the leaching test. Therefore, a sensitivity analysis has been performed on the main parameters that influence the hydro-geochemical behaviour of the compacted bentonite.

Regarding the initial water saturation of the compacted bentonite, as higher this parameter is, the higher the final amount of anhydrite precipitated close to the heater. This is mainly due to the fact that when the initial water saturation of the bentonite is higher there is more sulphate available to precipitate, because the sulphate concentration of the bentonite is higher than the sulphate concentration in the granite. As expected, higher initial amounts of Ca-sulphate in the bentonite, lead to higher anhydrite precipitated in the "warm" part of the bentonite. In addition, when the bentonite is considered to be initially free of Ca-sulphate minerals, the model predicts that under the themo-hydraulic conditions of the LOT A2 test, there is enough aqueous sulphate in the system for the accumulation of anhydrite close to the heater.

The increase of the water pressure applied at the granite boundary, from 1.2 MPa to 1.4 MPa, has very little effect on the final distribution of anhydrite. But, when this external water pressure is lower (1.0 MPa), the peak of total sulphate computed at the end of the experiment doubles that computed in the Base Case (1.2 MPa). In addition, in the case with a lower water pressure, there is less total sulphate in the "cold" area than in the Base Case. This is a consequence of the vapour condensation, which dilutes the concentration of solutes and dissolves the anhydrite previously precipitated.

The effect of diffusion coefficient indicates that for higher diffusivities more primary Ca-sulphate is dissolved, and consequently, higher amounts of aqueous sulphate are transported towards the evaporation front, where higher amounts of anhydrite precipitate.

Finally, the results for a low temperature (isothermal) case, also agrees very well with analytical data, indicating that the conceptual model used is applicable under a broad range of conditions. Main differences between this low temperature case and the thermal case are related to diffusivities, as high temperatures affect the water viscosity increasing the diffusivity in the system.

7 References

SKB's (Svensk Kärnbränslehantering AB) publications can be found at www.skb.se/publications.

Arcos D, Bruno J, Karnland O, 2003. Geochemical model of the granite-bentonite-groundwater interaction at the Äspö HRL (LOT experiment). Applied Clay Science, 23, pp 219–228.

Arcos D, Grandia F, Domènech C, 2006. Geochemical evolution of the near field of a KBS-3 repository. SKB TR-06-16, Svensk Kärnbränslehantering AB.

Arcos D, Grandia F, Domènech C, Fernández A M, Villar A M, Muurinen A, Carlsson T, Sellin P, Hernán P, 2008. Long-term geochemical evolution of the near field repository: insights from reactive transport modelling and experimental evidences. Journal of Contaminant Hydrology, 102, pp 196–209.

Birgersson M, Karnland O, 2009. Ion equilibrium between montmorillonite interlayer space and an external solution – Consequences for diffusional transport. Geochimica et Cosmochimica Acta, 73, pp 1908–1923.

Bourg I C, Sposito G, Bourg A C M, 2008. Modeling the diffusion of Na^+ in compacted water-saturated Na-bentonite as a function of pore water ionic strength. Applied Geochemistry, 23, pp 3635–3641.

Bradbury M H, Baeyens B, 2003. Porewater chemistry in compacted resaturated MX-80 bentonite. Journal Contaminant Hydrology, 61, pp 329–338.

González Sánchez F, Van Loon L R, Gimmi, T, Jakob, A, Glaus M A, Diamond L W, 2008. Self-diffusion of water and its dependence on temperature and ionic strength in highly compacted montmorillonite, illite and kaolinite. Applied Geochemistry, 23, pp 3840–3851.

Karnland O, Sandén T, Johannesson L E, Eriksen T E, Jansson M, Wold S, Pedersen K, Motamedi M, Rosborg B, 2000. Long term test of buffer material. Final report on the pilot parcels. SKB TR-00-22, Svensk Kärnbränslehantering AB.

Karnland O, Olsson S, Dueck A, Birgersson M, Nilsson U, Hernan-Hakansson T, Pedersen K, Nilsson S, Eriksen T-E, Rosborg B, 2009. Long-term test of buffer material at the Äspö Hard Rock Laboratory, LOT project. Final report on the A2 test parcel. SKB TR-09-29, Svensk Kärnbränslehantering AB.

Kozaki T, Liu J, Sato S, 2008. Diffusion mechanism of sodium ions in compacted montmorillonite under different NaCl concentration. Physics and Chemistry of the Earth, 33, pp 957–961 .

Kröhn K-P, 2003. New conceptual models for the resaturation of bentonite. Applied Clay Science, 23, pp 25–33.

Lasaga A C, Soler J M, Ganor J, Burch T E, Nagy K L, 1994. Chemical weathering rate laws and global geochemical cycles. Geochimica et Cosmochimica Acta, 58, pp 2361–2386.

Lerman A, 1971. Time to Chemical Steady-States in Lakes and Ocean. In: Hem J D (ed). Nonequilibrium systems in natural water chemistry. Washington, D.C.: American Chemical Society. Advances in Chemistry Series 106, pp 30–76

Leverett M C, 1941. Capillary behaviour in porous solids. Transactions of the Society of Petroleum Engineers of AIME, 142, pp 152–169.

Muurinen A, Karnland O, Lehikoinen J, 2004. Ion concentration caused by an external solution into the porewater of compacted bentonite. Physics and Chemistry of the Earth, 29, pp 119–127.

Ochs M, Talerico C, Sellin P, Hedin A, 2006. Derivation of consistent sorption and diffusion parameters and their uncertainties for compacted MX-80 bentonite. Physics and Chemistry of the Earth, 31, pp 600–609.

Olivella S, Gens A, Carrera J, Alonso, E-E, 1996. Numerical formulation for a simulator (CODE-BRIGHT) for the coupled analysis of saline media. Engineering Computations, 13, pp 87–112.

Parkhurst D L, Appelo C A J, 1999. User's guide to PHREEQC (Version 2) – A computer program for speciation, batch-reaction, one-dimensional transport, and inverse geochemical calculations: U.S. Geological Survey Water-Resources Investigations Report 99-4259.

Pruess K, Oldenburg C, Moridis G, 1999. TOUGH2 user's guide, Version 2.0, Lawrence Berkeley Laboratory Report LBL-43134, Berkeley, California.

Puigdomenech I, Ambrosi J-P, Eisenlohr L, Lartigue J-E, Banwart S A, Bateman K, Milodowski A E, West J M, Griffault L, Gustafsson E, Hama K, Yoshida H, Kotelnikova S, Pedersen K, Michaud V, Trotignon L, Rivas Perez J, Tullborg E-L, 2001. O_2 depletion in granitic media. The REX project. SKB TR-01-05, Svensk Kärnbränslehantering AB.

Schwartz F W, Zhang H, 2003. Fundamentals of groundwater. New York: Wiley.

SKB, 2004. Interim main report of the safety assessment SR-Can. SKB TR-04-11, Svensk Kärnbränslehantering AB.

Suzuki S, Sato H, Ishidera T, Fujii N, 2004. Study on anisotropy of effective diffusion coefficient and activation energy for deutrated water in compacted sodium bentonite. Journal of Contaminant Hydrology, 68, pp 23–37.

Tanikawa W, Shimamoto T, 2006. Klinkenberg effect for gas permeability an dits comparison to water permeability for porous sedimentary rocks. Hydrology and Earth System Sciences, 3, pp 1315–1338.

Udell K S, Fitch J S, 1985. Heat and mass transfer in capillary porous media considering evaporation, condensation, and non-condensible gas effects. Paper presented at 23rd ASME/AIChE National Heat Transfer Conference, Denver, Colorado.

Villar M V, Fernández A M, Gómez-Espina R, 2006. Effect of heating/hydration on bentonite: test in 60-cm long cell. CIEMAT/DMA/M2143/6/06, European Commission.

Villar M V, Fernández A M, Gómez R, Barrenechea J F, Luque F J, Martín P L, Barcala J M, 2007. State of a bentonite barrier after 8 years of heating and hydration in the Laboratory. In: Dunn D, Poinssot C, Begg B (eds). Scientific basis for nuclear waste management XXX. Warrendale, PA: Materials Research Society. (Materials Research Society Symposium Proceedings 985.)

Villar M V, Fernández A M, Martín P L, Barcala J M, Gómez-Espina R, Rivas P, 2008a. Effect of heating/hydration on compacted bentonite: tests in 60-cm long cells. Madrid: Ciemat.

Villar M V, Sánchez M, Gens A, 2008b. Behaviour of a bentonite barrier in the laboratory: Experimental results up to 8 years and numerical simulation. Physics and Chemistry of the Earth, 33, pp 476–485.

Wahlgren C-H, Curtis P, Hermanson J, Forssberg O, Öhman J, Fox A, La Pointe P, Drake H, Triumf C-A, Mattsson H, Thunehed H, Juhlin C, 2008. Geology Laxemar. Site descriptive modelling, SDM-Site Laxemar. SKB R-08-54, Svensk Kärnbränslehantering AB.

Wolery T J, 1992. EQ3/6, a computer program for geochemical aqueous speciation-solubility calculations: theoretical manual, user's guide, and related documentation (Version 7.0). Lawrence Livermore National Laboratory.

Wu Y-S, Pruess K, Persoff P, 1998. Gas flow in porous media with Klinkenberg effects. Transport in Porous Media, 32, pp 117–137.

Xu T, Pruess K, 2001. Modeling multiphase non-isothermal fluid flow and reactive geochemical transport in variably saturated fractured rocks: 1. Methodology. American Journal of Science, 301, pp 16–33.

Xu T, Sonnenthal E, Spycher N, Pruess K, 2008. TOUGHREACT User's guide: a simulation program for non-isothermal multiphase reactive geochemical transport in variably saturated geologic media. LBNL-55460, Lawrence Berkeley National Laboratory, University of California.

Åkesson M, Kristensson O, Börgesson L, Dueck A, Hernelind J, 2010. THM modelling of buffer, backfill and other system components. Critical processes and scenarios. SKB TR-10-11, Svensk Kärnbränslehantering AB.

Appendix A

Input files Base Case

Flow.inp

```
# axis-symmetric LOT experiment A2

# EOS1 flow input

ROCKS----1----*----2----*----3----*----4----*----5----*----6----*----7----*----8

BENT1    1     2750.       .43   1.0E-20   1.0E-20   1.0E-20      1.15      964.

                         1.0E+00    1.0E07

GRAN2    1     2750.    1.E-03   1.0E-20   1.0E-20   1.0E-20      1.15      964.

                                  1.0E07

CANI3    1     2750.       .43   1.0E-20   1.0E-20   1.0E-20      388.    1.E+20

                         1.0E+00    1.0E07

GRAN4    1     2750.    1.E-03   1.0E-20   1.0E-20   1.0E-20      1.15      964.

                         1.0E-09    1.0E07


MULTI----1----*----2----*----3----*----4----*----5----*----6----*----7----*----8

   2    3    2    8

REACT----1MOPR(20)-2----*----3----*----4----*----5----*----6----*----7----*----8

00020001

START----1----*----2----*----3----*----4----*----5----*----6----*----7----*----8

PARAM----1 MOP: 123456789*123456789*1234 ---*----5----*----6----*----7----*----8

  29999    90001100 30 0000002447115                  1.80

 0.000e00 3.1536E8  1.0E3       1.0E07                9.81

    1.E-5

         7.000E+04              0.5163              85.0

RPCAP----1----*----2----*----3----*----4----*----5----*----6----*----7----*----8

   5

   6        2.0E05    0.E-06       1.

TIMES----1----*----2----*----3----*----4----*----5----*----6----*----7----*----8

  11

  0.0     8.64E05  3.1536E06 6.3072E06  1.5800E7 1.8934E07 2.5246E07 3.1557E07
```

```
 7.844E07 1.5768E08  3.1536E8


INCON----1----*----2----*----3----*----4----*----5----*----6----*----7----*----8
A1  1
       7.00000E+04              0.5163     130.0
A11 3
       1.20000E+06               85.0
A11 4
       1.20000E+06               85.0
A11 5
       1.20000E+06               85.0
A11 6
       1.20000E+06               85.0
A11 7
       1.20000E+06               85.0
A11 8
       1.20000E+06               85.0
A11 9
       1.20000E+06               85.0
A1110
       1.20000E+06               85.0
A1111
       1.20000E+06              82.63
ENDCY----1----*----2----*----3----*----4----*----5----*----6----*----7----*----8
```

Solute.inp

‘LOT A2 experiment’

options for reactive chemical transport

2 1 5 0.00 0 2 2 0 0 ! ISPIA,INIBOUND,ISOLVC,rcour,NGAS1,ichdump,kcpl,lco2h2o,numdr

constraints for reactive chemical transport (4e10.4)

1.00e-4 0.000 4.0 1.0 !sl1min, d1min, stimax, cnfact

Read input and output file names:

ther_ympR4d.dat ! thermodynamic database

iter.dat ! iteration information

sca_conc.dat ! aqueous concentrations in tecplot form

sca_min.dat ! mineral data in tecplot form

sca_gas.dat ! gas data in tecplot form

time.dat ! concentrations at specific elements over time

Weighting parameters

1.0 1.0 3.0e-08 0.0 ! itime wupc,dffun,dffung

data for convergence criteria:

25 0.100E-03 50 0.100E-04 30 0.100E-05 0.00E-05 0.00E-05 ! ..... TOLDC,TOLDR

writing control variables:

1 1 10 4 1 0 2 ! NWTI,NWNOD,NWCOM,NWMIN,IWCOMT,iconflag(=1:mol/l),minflag(=1:Vf)

pointer of nodes for writing in time:

A1 3

pointer of components for writing:

3 4 5 6 7 8 9 10 11 12

pointer of minerals for writing:

1 2 3 4

default values of chemical zone codes for nodes: ! initial_water, boundary_water, minerals, gas, adsorb, exchan, permeab-porosi

1 1 1 1 0 0 1

chemical zone codes for nodes:

A1 1 0 0 1 0 0 0 0 2 1

A1 2 0 0 1 0 1 0 0 1 1

.

.

A11 2 0 0 1 0 1 0 0 1 1

A11 3 0 0 1 0 2 0 0 2 1

A11 4 0 0 2 0 2 0 0 2 1

.

.

A1110 0 0 2 0 2 0 0 2 1

A1111 0 0 2 1 2 0 0 2 1

nodes connected to gas supply (i.e.) atmosphere

end

Chemical.inp

LOT experiment

'----------'

'DEFINITION OF THE GEOCHEMICAL SYSTEM'

'PRIMARY AQUEOUS SPECIES'

'h2o'

'h+'

'ca++'

'mg++'

'na+'

'cl-'

'sio2(aq)'

'hco3-'

'so4--'

'k+'

'*'

'AQUEOUS COMPLEXES'

'oh-'

'cahco3+' ! Carbonates

'co2(aq)'

'caco3(aq)'

'nahco3(aq)'

'naco3-'

'mghco3+'

'mgco3(aq)'

'co3--'

'caoh+' ! Species with Ca

'caso4(aq)'

'kso4-' ! Species with K

'koh(aq)'

'mgso4(aq)' ! Species with Mg

‘mgoh+’

‘naoh(aq)’ ! Species with Na

’naso4-’

’hso4-’ ! Species with S(6)

’ca(h3sio4)2(aq)’ ! Species with Si

’cah2sio4(aq)’

‘cah3sio4+’

‘mg(h3sio4)2(aq)’

‘mgh2sio4(aq)’

‘mgh3sio4+’

‘*’

‘MINERALS’

‘anhydrite’ 0 0 0 0

0. 0. 0.

‘calcite’ 0 0 0 0

0. 0. 0.

‘sio2(am)_G’ 0 0 0 0

0. 0. 0.

‘gypsum’ 0 0 0 0

1. 0. 0.

‘*’ 0 0 0 0

‘GASES’

‘*’

‘SURFACE COMPLEXES’

‘*’

‘species with Kd and decay decay constant(1/s)’

‘*’ 0.0 0.0 0.0

‘EXCHANGEABLE CATIONS’ 0

‘ master convention ex. coef.’

‘na+’ 1 1 1.

‘k+’ 0 1 0.60

```
'ca++'          0          1          0.41
'mg++'          0          1          0.34
'*'             0          0          0.0
'------------------------------------------------------------------------'
'INITIAL AND BOUNDARY WATER TYPES'
2   1       !niwtype = number of initial waters, nbwtype = number of boundary waters
1    85.0                       !iwtype initial, temp (C)  BENTONITE POREWATER
'       icon       guess        ctot
'h2o'     1       1.000d+0      1.0000    ' ' 0.    ! kg water
'h+'      3       1.3836E-08    1.3836E-08  ' ' 0.    ! calculated from pH=7.859
'ca++'    1       1.0070E-02    1.0070E-02  ' ' 0.
'mg++'    1       5.8150E-03    5.8150E-03  ' ' 0.
'na+'     1       2.1190E-01    2.1190E-01  ' ' 0.
'cl-'     1       4.0000E-02    4.0000E-02  ' ' 0.
'sio2(aq)' 1       1.822e-003    1.822e-003  ' ' 0.    ! Unknown, taken from phreeqc eq. --> SiO2(am)
'hco3-'   1       1.0460E-03    1.0460E-03  ' ' 0.
'so4--'   1       9.6520E-02    9.6520E-02  ' ' 0.
'k+'      1       1.4050E-03    1.4050E-03  ' ' 0.
'*'       0       0.0           0.0       ' ' 0.
2    85.0                       !iwtype initial, temp (C)  ÄSPÖ GROUNDWATER
'       icon       guess        ctot        '
'h2o'     1       1.000d+0      1.0000    ' ' 0.    ! kg water
'h+'      3       1.2589E-07    1.2589E-07  ' ' 0.    ! calculated from pH=6.9 at 25C  (1.2589E-7)
'ca++'    2       5.6000E-02    5.6000E-02  'anhydrite' -0.49
'mg++'    1       1.6000E-03    1.6000E-03  ' ' 0.
'na+'     1       9.6000E-02    9.6000E-02  ' ' 0.
'cl-'     1       1.7800E-01    1.7800E-01  ' ' 0.
'sio2(aq)' 1       1.6000E-04    1.6000E-04  ' ' 0.
'hco3-'   1       4.4000E-04    4.4000E-04  ' ' 0.
'so4--'   1       6.0000E-03    6.0000E-03  ' ' 0.
'k+'      1       2.6000E-04    2.6000E-04  ' ' 0.
```

```
'*'       0        0.0          0.0        ' ' 0.
1    85.0                        !iwtype initial, temp (C)  ÄSPÖ GROUNDWATER
'       icon       guess        ctot        '
'h2o'     1       1.000d+0      1.0000     ' ' 0.     ! kg water
'h+'      3       1.2589E-07    1.2589E-07  ' ' 0.     ! calculated from pH=6.9 at 25C  (1.2589E-7)
'ca++'    2       5.6000E-02    5.6000E-02  'anhydrite' -0.49
'mg++'    1       1.6000E-03    1.6000E-03  ' ' 0.
'na+'     1       9.6000E-02    9.6000E-02  ' ' 0.
'cl-'     1       1.7800E-01    1.7800E-01  ' ' 0.
'sio2(aq)' 1      1.6000E-04    1.6000E-04  ' ' 0.
'hco3-'   1       4.4000E-04    4.4000E-04  ' ' 0.
'so4--'   1       6.0000E-03    6.0000E-03  ' ' 0.
'k+'      1       2.6000E-04    2.6000E-04  ' ' 0.
'*'       0        0.0          0.0        ' ' 0.
'-------------------------------------------------------------------------------'
'INITIAL MINERAL ZONES'
 2
 1                          ! bentonite
'mineral         vol.frac.    propyllytic/phyllic zone'
'anhydrite'   0.0015  0
'calcite'     0.000  0
'sio2(am)_G'   0.052  0
'gypsum'      0.000  0                                    ! 'gypsum'      0.008  0
'*'           0.0    0
 2
'mineral         vol.frac.    propyllytic/phyllic zone'
'*'           0.0    0
'-------------------------------------------------------------------------------'
'INITIAL gas ZONES'
1                           !ngtype= number of gas zones
1                           !igtype
```

‘gas partial pressure’ !at 25 C equil w/ water

‘*’ 0.0

‘----------’

‘Permeability-Porosity Zones’

1

1

‘perm law a-par b-par tcwM1’

1 0.0 0.0 ! 5 0.46 10.0 ! PHIc=0.46, n(power term)=10

‘----------’

‘INITIAL SURFACE ADSORPTION ZONES’

0 !ndtype= number of sorption zones

‘zone ad.surf.(m2/kg) total ad.sites (mol/l)’

‘----------if Sden=0 Kd store retardation factor’

‘INITIAL LINEAR EQUILIBRIUM Kd ZONE’

1 !kdtpye=number of Kd zones

1 !idtype

‘species solid-density(Sden,kg/dm**3) Kd(l/kg=mass/kg solid / mass/l’

‘*’ 0.0 0.0

‘----------if Sden=0 Kd store retardation factor’

‘INITIAL ZONES OF CATION EXCHANGE’

2 !nxtype= number of exchange zones

‘zone ex. capacity’

1 75. ! 75 meq/100 g of bentonite

2 1.E-95

‘----------’

‘en